Earth-Science Reviews 246 (2023) 104574

Contents lists available at ScienceDirect

Earth-Science Reviews

journal homepage: www.elsevier.com/locate/earscirev

Bias in sediment chemical weathering intensity evaluation: A numerical simulation study

Hanjing Fu[a], Xing Jian[a,*], Hanqing Pan[b]

[a] State Key Laboratory of Marine Environmental Science, College of Ocean and Earth Sciences, Xiamen University, Xiamen 361102, PR China
[b] School of Aerospace Engineering, Xiamen University, Xiamen 361102, PR China

ARTICLE INFO

Keywords:
Chemical weathering intensity
Major elements indices
Mineral composition
Grain size
Sediment source-to-sink system

ABSTRACT

Silicate weathering is critical to global carbon cycle and climate change, and has attracted considerable attention in Earth science studies. Chemical weathering intensity evaluation and paleoclimatic reconstruction based on siliciclastic sediment composition analysis are popular topics. However, chemical weathering signals are difficult to be accurately extracted from sediment compositions due to multiple, complex processes and factors in sediment source-to-sink systems. To better understand the bias in evaluation of chemical weathering intensity, we conduct Monte Carlo simulations to explore the relationships between sediment compositions and widely-used major elements-based weathering indices, i.e., Chemical Index of Alteration (CIA), Chemical Index of Weathering (CIW), Plagioclase Index of Alteration (PIA), Weathering Index of Parker (WIP), the modified CIA (CIX) and representative element ratios (i.e., K/Al, Na/Al, Na/K, SiO_2/Al_2O_3). Most chemical weathering indices are dominated by the total clay mineral content in sediments and exhibit remarkable grain size bias from hydrodynamic sorting, manifesting by variations of ca. 20 in CIA, CIW, PIA, WIP and CIX values between simulated sandy (15 wt% clay minerals) and muddy (47 wt% clay minerals) sediments. Clay mineral species, which might be shaped by source lithology, climate and even diagenesis, display noticeable effects to weathering indices in clay mineral-rich sediments. Although the plagioclase/K-feldspar ratios almost have no influence on CIA, the effects of detrital feldspar types and abundances are prominent on most weathering indices. Thus, source lithological bias cannot be overlooked in sediment weathering intensity evaluation under various climatic conditions because of the significant lithology controls on feldspar fertility and clay mineral species. The WIP and SiO_2/Al_2O_3 indices are highly sensitive to quartz contents (e.g., quartz/feldspar ratios), which are closely related to sediment recycling and source lithology. This study, from the numerical simulation perspective, provides quantitative insight into biases in sediment chemical weathering intensity evaluation. Our findings highlight the importance of a comprehensive understanding how the sediment source-to-sink processes and factors influence siliciclastic sediment compositions, textures and chemical weathering indices. We advocate that a systematic analysis (e.g., mineralogy, grain size, provenance, etc.) on targeted sediments or sedimentary rocks is necessary for interpreting sedimentary weathering records.

1. Introduction

Continental chemical weathering is considered as a critical process in shaping the Earth's surface morphology, connecting the atmosphere-hydrosphere-lithosphere systems, constituting carbon biogeochemical cycles, supplying nutrients to ecosystems and regulating global climate (West et al., 2005; Liu et al., 2011). Rising atmospheric CO_2, as a major factor of global warming, can be consumed by silicate chemical weathering by precipitation as carbonate buried in oceans, and eventually cooling down the global temperature (Millot et al., 2002; Penman et al., 2020). This kind of negative feedback mechanism between silicate weathering and atmospheric CO_2 concentrations in the Earth's history contributes to global climate stability and plays an important role in maintaining the Earth's habitability over geological timescales (Maher and Chamberlain, 2014; Arnscheidt and Rothman, 2022). Deep-time silicate chemical weathering studies help to understand paleoclimate change, implicating for both the current global climate change and future climate tendency (White and Brantley, 2018). Therefore, continental silicate chemical weathering intensity and rate, mechanism and evolution are hot topics in Earth sciences and have attracted

* Corresponding author.
E-mail address: xjian@xmu.edu.cn (X. Jian).

https://doi.org/10.1016/j.earscirev.2023.104574
Received 15 February 2023; Received in revised form 22 September 2023; Accepted 25 September 2023
Available online 28 September 2023

considerable attentions for decades.

Chemical weathering decomposes and alters primary minerals in fresh rocks by CO_2, O_2 and water, accompanied by formation of secondary minerals (Penman et al., 2020). Soluble and mobile elements (e.g., K, Na, Ca and Mg) are easily depleted and tend to be dissolved in water during the weathering processes, whereas immobile and non-soluble elements (e.g., Al, Fe and Ti) are enriched in weathering residues (Buggle et al., 2011; Perri, 2020). Thus, mineralogical and chemical compositions of weathering products and residues can preserve weathering signals (Hu et al., 2016; Dinis et al., 2020). Fluvial and lacustrine sediments/sedimentary rocks and other targets (e.g., marine carbonates, paleo-soils and paleo-weathering profiles), composed of weathering products and residues, are widely investigated to evaluate continental silicate weathering intensities and patterns over multiple temporal-spatial scales in combination with a variety of proxies (e.g., Yang et al., 2004; Shao et al., 2012; Zhao and Zheng, 2015; Zhai et al., 2018; Lv et al., 2022). Numerous geochemical indices have been proposed based on the weathering properties of silicate-bound elements (Gupta and Rao, 2001; Price and Velbel, 2003). Major element-based indices include dual-elemental indices (e.g., K/Al, Na/Al, Na/K, Ca/Ti, SiO_2/Al_2O_3, Ruxton, 1968; Burke et al., 2007; Hu et al., 2016) and multi-elemental indices, e.g., the Chemical Index of Alteration (CIA; Nesbitt and Young, 1982), the Chemical Index of Weathering (CIW; Harnois, 1988), the Plagioclase Index of Alteration (PIA; Fedo et al., 1995), the Weathering Index of Parker (WIP; Parker, 1970) and the modified CIA (CIX; Garzanti et al., 2014). These multi-elemental weathering indices are popularly used to quantitatively document variations in paleo-weathering intensity and paleoclimate (e.g., Li and Yang, 2010; Clift et al., 2014; Zhao and Zheng, 2015; Nadłonek and Bojakowska, 2018; Cao et al., 2019). However, growing studies have shown that these indices have obvious limitations in evaluating chemical weathering intensity of siliciclastic sediments and sedimentary rocks, which may result in misinterpretations of paleoclimate and paleoenvironment changes (Shao et al., 2012; Guo et al., 2018; Ren et al., 2019). For example, grain size differentiation of sediments/sedimentary rocks used in case studies leads to incomparably different values of weathering indices, even though samples with different grain sizes are subjected to similar intensity of chemical weathering (Jian et al., 2013; Zhang et al., 2021a).

Except for the chemical weathering process, other processes in sediment source-to-sink systems (Fig. 1), such as source material supply, hydrodynamic sorting during transport and deposition, post-depositional diagenesis and sediment recycling, shape mineralogical and chemical compositions of siliciclastic sediments to different extent and thus complicate weathering intensity evaluation (Fedo et al., 1995; von Eynatten, 2004; Bouchez et al., 2011; Garzanti et al., 2011; Joo et al., 2018). Sediments derived from felsic-, mafic- crystalline rocks or recycled sedimentary rocks produce different primary mineral and secondary mineral species (Fig. 1, von Eynatten et al., 2012; Chetelat et al., 2013). Polycyclic sedimentary rocks have cumulative effect from sedimentary cycles and tend to accumulate stable minerals (e.g., quartz), which can significantly affect the utility of quartz dilution-sensitive indices (e.g., WIP) (Garzanti et al., 2013a; Yang et al., 2016; Dinis et al., 2017; Guo et al., 2017). Source rock lithology bias commonly exist in evaluation of paleo-weathering intensity for sedimentary rock samples due to the uncertain source terranes and paleogeographic frameworks (Dinis et al., 2017; Cao et al., 2019). During the transport and deposition processes, mineral particles with the same settling velocity are gathered in specific sediment fractions based on grain size, shape and density (Garzanti et al., 2010, 2011). The mineralogical and chemical differentiation of sediments induced by hydrodynamic sorting leads to a strong correlation of geochemical indices (e.g., CIA) with grain size, i.e., so-called grain size effect (Xiong et al., 2010; Shao et al., 2012; Jian et al., 2013; Guo et al., 2018; Zhang et al., 2021a). A variety of mineral transformations may occur in diagenesis processes, e.g., kaolinite and smectite illitization, and thus affect chemical element concentrations in sedimentary rocks (Fedo et al., 1995; Buggle et al., 2011; Dinis et al., 2020). These processes may obscure climate-controlled weathering signals in sediments, decoupling chemical weathering indices values from the objective climatic conditions. The effects from external interferences and related sediment composition changes on weathering indices have not yet been systematically elucidated and specifically quantified. The above-mentioned biases have been realized in many case studies, however, how to quantitatively analyze these biases and reduce misleading interpretations remains an open question.

In this study, we focus on the commonly-used major elemental indices (i.e., CIA, CIW, PIA, WIP, CIX, K/Al, Na/Al, Na/K, SiO_2/Al_2O_3) and investigate the influences of variable sediment compositions on weathering indices through Monte Carlo simulation test. The major purposes are (1) to quantify the influence of sediment mineral compositions and grain size on these indices; (2) to evaluate the applicable conditions of these weathering indices; (3) to review the interferences in sediment source-to-sink processes on weathering intensity evaluation.

2. Chemical weathering indices: a review

The CIA proxy was pioneered by Nesbitt and Young (1982) for quantitative assessment of chemical weathering intensity as represented by the degree of feldspar alteration, and has become the most popular indicator (Li and Yang, 2010; Deng et al., 2022). The definition of CIA (formula refers to Table 1) is based on the molar proportions of silicate-bound major elements (i.e., Al, K, Ca and Na). In the calculation formula, CaO* represents the CaO associated with silicate component of the analyzed samples. For sedimentary samples, the CaO* content is commonly evaluated by either of two methods, i.e., measuring sediment CaO concentration after acid-treatment for removing of Ca in carbonate and phosphate (Pang et al., 2018), or empirical calculation involving the CaO/Na_2O ratio in silicate minerals (McLennan, 1993). In the second method, n(CaO*) can be expressed by n(CaO) if $n(CaO) \leq n(Na_2O)$, or n(CaO*) is assigned as $n(Na_2O)$ when $n(CaO) > n(Na_2O)$ (n represents the mole content). To avoid the interference of carbonate on evaluation of weathering intensity, Garzanti et al. (2014) proposed the CIX index by modification of the CIA formula where element Ca is not involved. In order to avoid the effect of inconsistent geochemical behaviour of potassium during weathering process, Harnois (1988) proposed the CIW proxy by eliminating K_2O from the CIA equation (Table 1). Even so, it is proved that K-feldspar-rich sediments are expected to have high CIW values, regardless of weathering intensity. Fedo et al. (1995) subsequently defined the PIA proxy as an alternative to CIA and CIW after adjusting the calculation of elements Al and K in formula (Tunçay et al., 2019; Dinis et al., 2020). The above-mentioned geochemical indices are based on the relative ratios of both mobile and immobile elements, however, the WIP proxy proposed by Parker (1970) only focuses on the absolute concentrations of mobile elements bound to silicates (Table 1). The calculations of CIA, CIW, PIA, WIP, CIX indices are based on the ratio of element concentration with the same unit, and then multiplied by 100 (Table 1). Thus, the units of CIA, CIW, PIA, WIP, CIX are in percent (%) and are omitted in this paper for simplified expressions. Except for CIA, CIW, PIA, WIP and CIX, the dual-elemental ratios including K/Al, Na/K, Na/Al and SiO_2/Al_2O_3 (Ji et al., 2004) are also employed in our numerical simulation tests.

Our study mainly focuses on the major-elemental indices mentioned above. Popular chemical weathering indicators also include trace-elemental indices, for example, Rb/Sr and α_E^{Al}. Elements Rb and Sr are mainly hosted in K-bearing minerals (e.g., K-feldspar, biotite and muscovite) and Ca-bearing minerals (e.g., plagioclase, pyroxene, amphibole and carbonate), respectively. Due to the preferential weathering of Ca-bearing (Sr-rich) minerals, element Sr tends to be depleted and Rb/Sr ratio increases with enhancement of chemical weathering intensity (Jin et al., 2006; Chang et al., 2013). α_E^{Al} is a ratio of mobile element E (e.g., Mg, Ca, Na, Sr, K, Ba) and immobile element Al

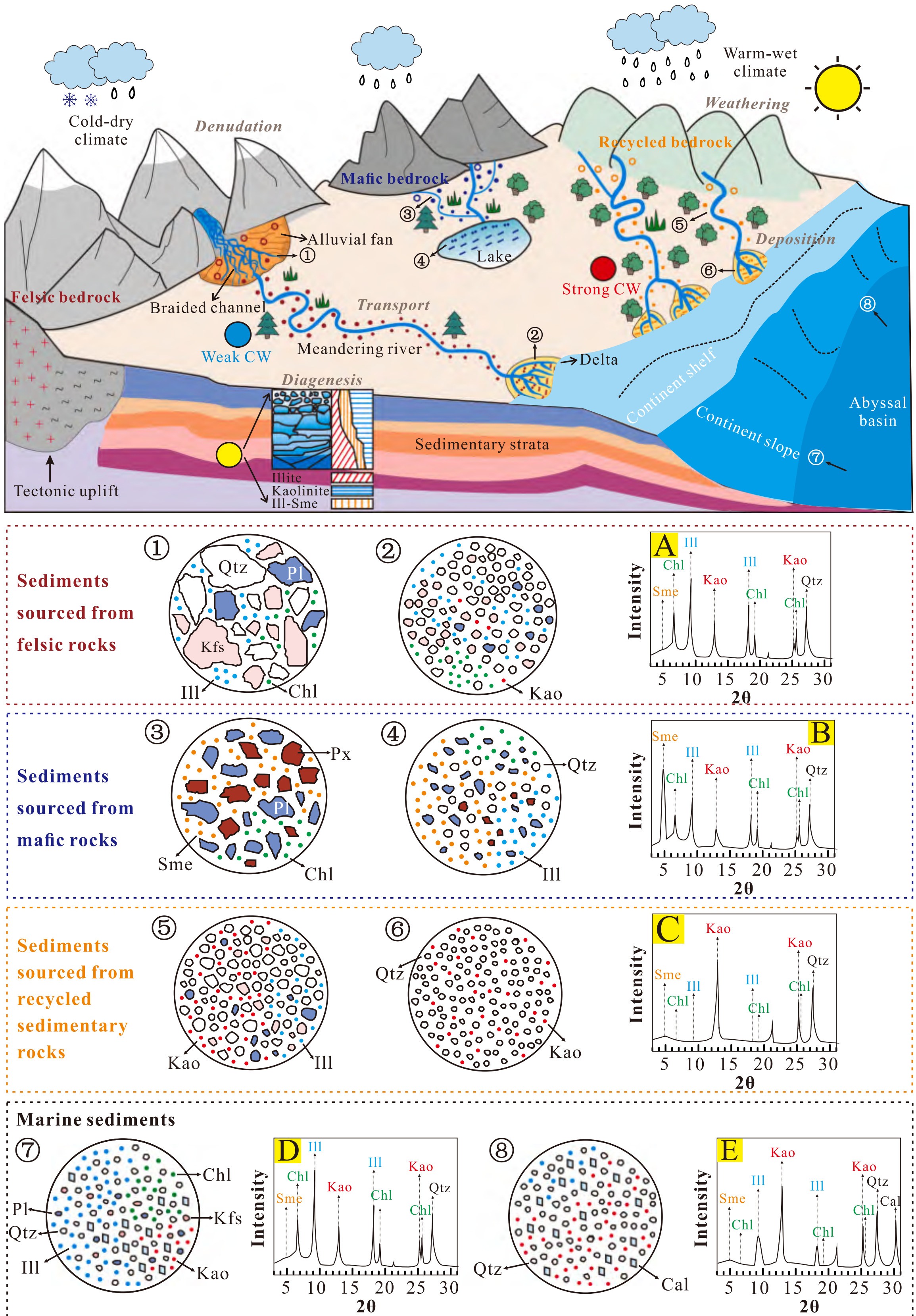

(caption on next page)

Fig. 1. Typical sediment compositions throughout the sediment source-to-sink system. Processes and factors in source-to-sink system include source rock lithology, climate, physical denudation, chemical weathering, sediment transport, deposition and diagenesis. Source bedrock lithologies: felsic-, mafic- igneous (red cross) rocks, metamorphic (black wave) rocks and sedimentary rocks. Strong chemical weathering (red dot) under warm-wet climate is shown in right side and weak chemical weathering (blue dot) under cold-dry climate is shown in left side. Chemical weathering is short for CW. Hydrodynamic sorting during sediment transport differentiates mineral compositions of sediment fractions with different grain sizes (conglomerate: hollow circle, sand: solid dot, silt: dual-dots, mud: short line). Quartz and feldspars are accumulated in coarse-grained sediments, and phyllosilicate minerals are accumulated in fine-grained sediments. Kaolinite illitization related to post-deposited diagenesis (yellow dot) changes clay mineral content and species. Schematic diagrams of petrological photos of sediments generated from different environments are shown in ①–⑧. Quartz (Qtz): white; K-felspar (Kfs): pink; Plagioclase (Pl): blue-purple; Pyroxene (Px): red-brown; Illite (Ill): blue dot; Chlorite (Chl): green dot; Kaolinite (Kao): red dot; Smectite (Sme): orange dot; Calcite (Cal): white diamond. ①: quartz and K-feldspar dominant, coarse and angular grains, poor sorting; ②: quartz and illite dominant, fine and round grains, well sorting; ③: pyroxene and plagioclase dominant, moderately coarse and angular grains, moderate sorting; ④: plagioclase and smectite dominant, fine and subangular-subrounded grains, moderate sorting; ⑤: quartz and kaolinite dominant, moderately coarse and subrounded grains, moderate sorting; ⑥: quartz and kaolinite dominant, fine and round grains, well sorting; ⑦: quartz and illite dominant, minor amounts of marine authigenic carbonate, fine and round grains, well sorting; ⑧: quartz and kaolinite dominant, minor amounts of authigenic carbonate, fine and round grains, well sorting. Figs. A (samples 1 and 2), B (samples 3 and 4), C (samples 5 and 6), D (sample 7), E (sample 8) show X-ray diffraction patterns of clay mineral assemblages in sediments. (For interpretation of the references to colour in this figure legend, the reader is referred to the web version of this article.)

Table 1
Summary of weathering indices in this study.

Indicators	Formula and references	Value ranges in sediments	Pl	Kfs	Kao	Ill	Chl	Sme	Bt	Ms	Px	Ol	Hbl	PAAS	NASC	UCC
Chemical Index of Alteration (CIA)	CIA = Al_2O_3 / (Al_2O_3 + K_2O + CaO* + Na_2O) × 100; Nesbitt and Young, 1982, 1989	100–50	50	50	100	68	100	83	50	75	17	–	30	70	68	48
Chemical Index of Weathering (CIW)	CIW = Al_2O_3 / (Al_2O_3 + CaO* + Na_2O) × 100; Harnois, 1988	100–40	50	100	100	100	100	83	100	100	17	–	30	83	82	54
Plagioclase Index of Alteration (PIA)	PIA = (Al_2O_3 - K_2O) / (Al_2O_3 - K_2O + CaO* + Na_2O) × 100; Fedo et al., 1995, 1996	100–50	50	–	100	100	100	83	–	100	17	–	30	79	77	47
Weathering Index of Parker (WIP)	WIP = (CaO* / 0.7 + 2Na_2O / 0.35 + 2K_2O / 0.25 + MgO / 0.9) × 100; Parker, 1970	≥100–0	79	144	0	70	70	13	156	100	109	116	30	51	55	80
the modified CIA (CIX)	CIX = Al_2O_3 / (Al_2O_3 + K_2O + Na_2O) × 100; Garzanti et al., 2014	100–50	75	50	100	68	100	91	50	75	80	–	100	76	73	60

Notes: parameters in formulas use molecular proportions. CaO* is CaO bound to silicate component in the sediment. PAAS: post-Archean Australian Average Shale. NASC: North American Shale Composite. UCC: Upper Continental Crust. Geochemical data of PAAS and UCC refer to Taylor and McLennan (1985) and geochemical data of NASC refer to Gromet et al. (1984). Pl: plagioclase, Kfs: K-feldspars, Kao: kaolinite, Ill: illite, Chl: chlorite, Sme: smectite, Bt: biotite, Ms.: muscovite, Px: pyroxene, Ol: olivine, Hbl: hornblende. Ideal chemistries of typical minerals are referenced from the "RRUFF Project" website (https://rruff.info/) and "X-Ray Diffraction Table" website (http://webmineral.com/MySQL/xray.php#.ZFNCZyIsa_c).

in sediments normalized to the UCC (Upper Continental Crust) composition, with the calculation formula of $\alpha_E^{Al} = (Al/E)_{sample}/(Al/E)_{UCC}$ (Garzanti et al., 2013b). $\alpha_E^{Al} > 1$ represents that the elements are reduced in sediments relative to UCC due to weathering (Gaillardet et al., 1999). Additionally, mineralogical indicators, i.e., the clay mineral assemblages and contents, and their crystallization characteristics (illite crystallinity and illite chemistry index, Esquevin, 1969; Ehrmann, 1998), are widely used to reconstruct weathering intensity and paleoclimate from the perspective of weathering products. Stable isotopic indices (e.g., $^{87}Sr/^{86}Sr$, δ^7Li, $\delta^{11}B$, $\delta^{41}K$, $\delta^{26}Mg$ and $\delta^{30}Si$) developed in recent years show high potentials to quantitatively evaluate chemical weathering intensity (Opfergelt and Delmelle, 2012; Opfergelt et al., 2012; Millot et al., 2019; Teng et al., 2020).

3. Numerical simulation methodology

Quartz (Qtz), plagioclase (Pl) and K-feldspar (Kfs) constitute 70%–80% of the upper crust and are major minerals of siliciclastic sediments (Nesbitt et al., 1997). These minerals are important parameters for numerical simulations. Kaolinite (Kao), illite (Ill), chlorite (Chl) and smectite (Sme) are involved in numerical simulations as typical clay minerals. Chemical formulas of these typical minerals (Table 2) are cited from the "RRUFF Project" (https://rruff.info/) and the "X-Ray Diffraction Table" (http://webmineral.com/MySQL/xray.php#.ZFNCZyIsa_c) websites. Although lithic fragments are common components in sandy siliciclastic sediments, the components can be regarded as aggregates of the above minerals and thus are not concerned in our simulation. Other minerals, such as muscovite, biotite and heavy minerals (e.g., tourmaline, garnet, epidote, hornblende, pyroxene), are not considered in simulation for their low absolute contents in sediments or occurrence only under certain conditions (Garzanti and Andò, 2019).

Table 2
Chemical formulas of minerals used as simulation parameters.

Minerals	Abbreviations	Ideal chemistry
Quartz	Qtz	SiO_2
Plagioclase	Pl	$Na_{0.5}Ca_{0.5}Si_{2.5}Al_{1.5}O_8$
K-feldspar	Kfs	$KAlSi_3O_8$
Kaolinite	Kao	$Al_2Si_2O_5(OH)_4$
Illite	Ill	$K_{0.6}(H_3O)_{0.4}Al_{1.3}Mg_{0.3}Fe^{2+}_{0.1}Si_{3.5}O_{10}(OH)_2(H_2O)$
Chlorite	Chl	$Mg_{3.75}Fe^{2+}_{1.25}Si_3Al_2O_{10}(OH)_8$
Smectite	Sme	$Na_{0.2}Ca_{0.1}Al_2Si_4O_{10}(OH)_2(H_2O)_{10}$

Notes: Chemical formulas of minerals are cited from the "RRUFF Project" (https://rruff.info/) and "X-Ray Diffraction Table" (http://webmineral.com/MySQL/xray.php#.ZFNCZyIsa_c) websites. Therein, mineral chemical compositions of K-feldspar, smectite and chlorite refer to the entry "orthoclase", "montmorillonite" and "clinochlore" in https://rruff.info/, respectively.

Here, we use Monte Carlo simulation method to quantitatively model each mineral proportion under different clay mineral content conditions with randomly sampled 100,000 times in uniform probability distributions. The simulation is designed to analyze the effect of mineral ratio changes, and satisfies the conditions shown in Table 3-1. The mean values and standard deviations of seven minerals concentrations indicate that simulated data meet uniform distribution (Table A1), revealing high robustness of Monte Carlo simulation results.

To investigate grain size bias in sediment chemical weathering intensity evaluation, here the simulated sediments are simply lithologically classified as sandy, silty and muddy sediments, with mean grain sizes in 63 μm–2 mm, 4–63 μm, <4 μm, respectively. It is well known that grain size-related lithological classification for natural clastic rocks (e.g., sandstone and mudstone) is closely related to the clay mineral content therein (Di Stefano et al., 2010; Guo et al., 2018; Warr, 2022). Thus, clay mineral content is used to represent a parameter for distinguishing simulated sediment lithology in this study (i.e., grain size differences). We collect bulk mineralogical data from published studies and posit that the average clay mineral contents in sandy, silty and muddy sediments and sedimentary rocks are ca. 15 wt%, 38 wt% and 47 wt% (weight percentage), respectively (Fig. A1, Battaglia et al., 2003; Tolosana-Delgado and von Eynatten, 2009; Garzanti et al., 2011; von Eynatten et al., 2012; Zhou et al., 2015; Guo et al., 2018; Wu et al., 2019; Chen et al., 2020a; Jian et al., 2020). Big data analysis results (Warr, 2022) indicate that sandstones ($n = 1112$, n is short for the number of samples) and low permeability rocks (including mudstone, siltstone, shales and phyllites, $n = 3186$) contain 15 wt% and 46 wt% clay minerals on average, respectively, revealing that our assumption is robust. Although in some cases, there are negative correlations between feldspar content and clay mineral content (sediment grain size) (Tolosana-Delgado and von Eynatten, 2009; Lai et al., 2015; Li et al., 2019d; Jian et al., 2020; Ma et al., 2022). The collected bulk mineralogical data show that feldspar content does not strictly decrease with the increase of clay mineral content or decline of sediment grain size (Fig. A1; Yuste et al., 2004). In order to explore the responses of chemical weathering indices values to grain size effect, we set up two experimental conditions for simulation test, i.e., (1) the non-correlation between feldspar and clay mineral content (absolutely random) and (2) the negative correlation between feldspar and clay mineral content. Mineral compositions are randomly sampled with clay mineral content varying from 0 to 100 for 200,000 times under the first condition (non-correlation) and for 100,000 times under the second condition (negative correlation) by Monte Carlo simulations. Mineralogical data generally meet uniform distributions (Table A2). Parameter setting is shown in Table 3-2.

Table 3
Monte Carlo simulation of sediment mineral composition and grain size changes: parameter settings.

(1) Effects of mineral ratio changes on weathering indices values

Variate 1	Variate 2	Other parameters
Kao/Ill = 0–20 Kao/Sme = 0–20 Pl/Kfs = 0–20 Qtz/Fsp = 0–20	CMC = 10 wt%, 50 wt%, 90 wt%	Avg. Qtz = Pl = Kfs = (100-CMC)/3; Avg. Kao = Sme = Ill = Chl = CMC/4

(2) Effects of grain size changes on weathering indices values

Conditions	Variate	Other parameters	Grain size differentiation
Non-correlation	CMC = 0–100 wt%	Avg. Qtz = Pl = Kfs Avg. Kao = Sme = Ill = Chl	Sand: Avg. CMC = 17 wt%; Silt: Avg. CMC = 43 wt%; Clay: Avg. CMC = 54 wt%
Negative correlation	CMC = 0–20 wt%, Fsp = 40–50 wt%; CMC = 20–40 wt%, Fsp = 30–40 wt%; CMC = 40–60 wt%, Fsp = 20–30 wt%; CMC = 60–80 wt%, Fsp = 10–20 wt%; CMC = 80–100 wt%, Fsp = 0–10 wt%	Avg. Pl = Kfs Avg. Kao = Sme = Ill = Chl	

Notes: The description of mineral abbreviations is shown in caption of Table 2. The sum of Qtz, Pl, Kfs, Kao, Ill, Sme and Chl is 100 wt%. CMC: clay mineral content, sum of the contents of kaolinite, illite, smectite and chlorite. Fsp: feldspar, sum of the contents of plagioclase and K-feldspar. Avg: it represents the average value of randomly sampled data of a mineral. Parameters conform to uniform distribution. The Kao/Ill, Kao/Sme, Pl/Kfs and Qtz/Fsp ratios set in the range of 0–20 are suitable for most situations.

4. Sensitivity of chemical weathering indices to changes in sediment mineral compositions

4.1. Total clay mineral content dominates most weathering indices

Clay minerals in siliciclastic sediments and sedimentary rocks are widely used to constrain paleo-weathering intensity and paleoclimate evolution (e.g., Wang et al., 2015; Liu et al., 2016b; Yu et al., 2016; Dianto et al., 2019; Liu et al., 2020). However, it is worth noting that clay mineral contents in first-cycle sediments are not only controlled by climate-dominated source chemical weathering (Egli et al., 2001; Yusoff et al., 2013; Liu et al., 2016a) but also by hydrodynamic sorting during sediment transport and deposition processes. Detrital grains experience grain size differentiation in hydrodynamic sorting, in which clay minerals tend to accumulate in fine-grained sediments (Fig. A1) due to their small size, platy shape and low density (Nesbitt et al., 1996; Repasch et al., 2022). Several case studies demonstrate that, under the same chemical weathering condition, weathering indices values of fine-grained sediments (e.g., higher CIA and lower WIP values) are different from those of coarse-grained sediments (Jian et al., 2013; Zhang et al., 2021a).

The grain size bias is confirmed and quantified in our numerical simulation study. Results show that most chemical weathering indices are dominated by total clay mineral contents in sediments (Fig. 2, Fig. A2). The decrease of grain size leads to increases of CIA, CIX, CIW and PIA values and decreases of WIP, K/Al, Na/Al values, whereas Na/K and SiO_2/Al_2O_3 ratios have obscure responses to grain size changes (Fig. 2, Fig. A2). The difference of CIA values between simulated sandy (defined by using the average clay mineral content of 15 wt%, the same hereinafter) and muddy (47 wt%) sediments reaches to ca. 15, and that is approximately 10 for CIX index (Fig. 2). Compared with the absolutely random ("non-correlation") simulation (Table 3), the "negative correlation" simulation results (Fig. A3) show similar response patterns of chemical weathering indices values to sediment grain size changes, especially for CIA, CIX, CIW, PIA, K/Al, Na/Al and Na/K indices (Fig. 2, Fig. A2, Fig. A3). Therefore, the analysis and interpretation of grain size effect in this work are mainly based on the results of the "non-correlation" simulation test. Additionally, abundance and species of felspars in sediments may enlarge or shrink the variation ranges of CIW, PIA, WIP, SiO_2/Al_2O_3, K/Al, Na/Al and Na/K values induced by grain size variations (Fig. 2, Fig. A2). Compared with the "non-correlation" simulation test, the "negative correlation" simulation test results show that the influences of feldspar content on SiO_2/Al_2O_3 and WIP indices are relatively slighter (Fig. A3, Fig. 2), because this test has considered the potential linkages between feldspar content and clay mineral content in sediments. Considering synergistic effects of feldspar and clay minerals enhances the grain size effect on WIP values with a variation range of ca. 20 (Fig. A3). Overall, these results demonstrate that the total clay mineral content in siliciclastic sediments is the most essential factor for quantitatively evaluating chemical weathering intensity.

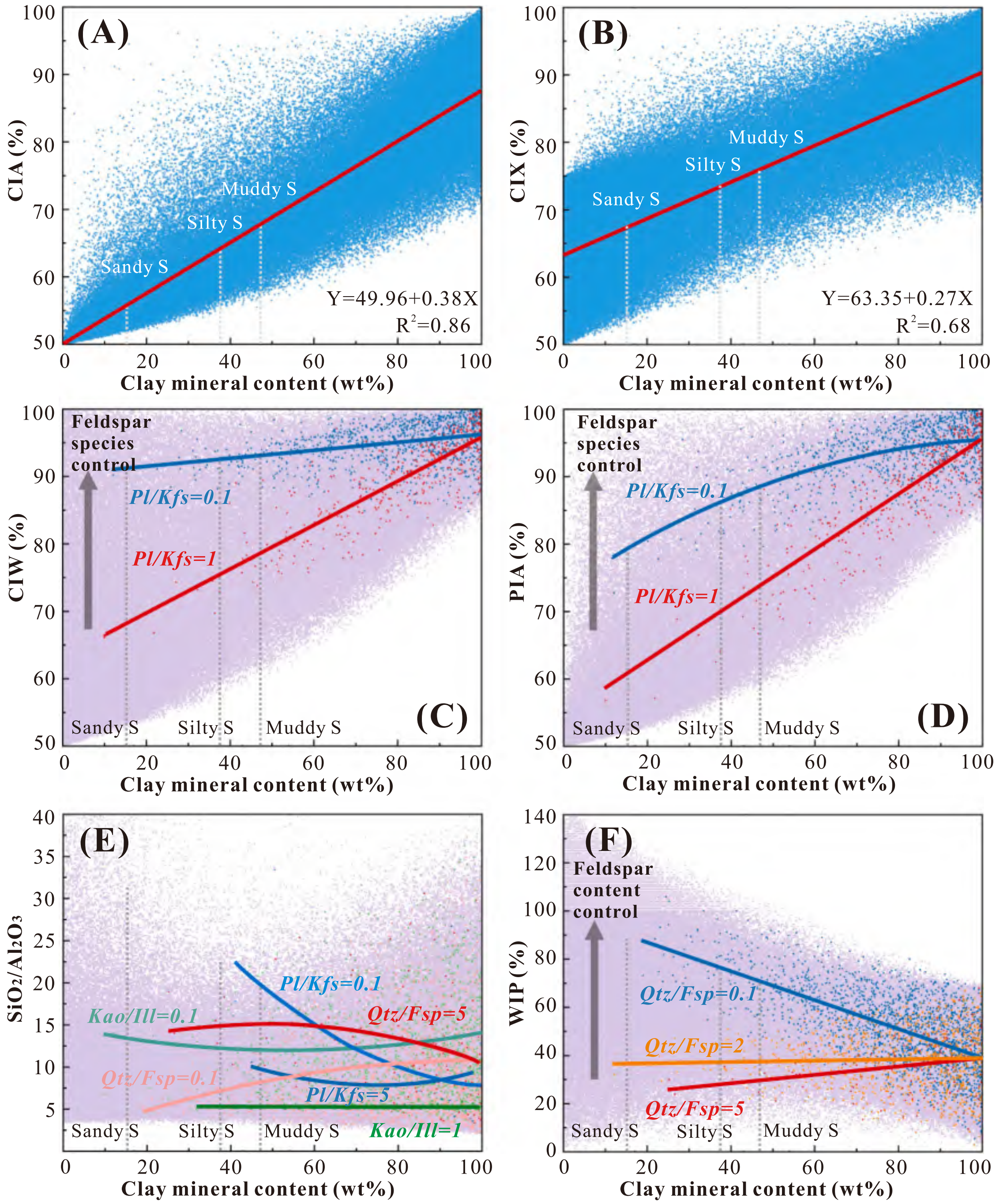

Fig. 2. Correlations between CIA, CIX, CIW, PIA, SiO_2/Al_2O_3, WIP values and total clay mineral content in sediments. The average of clay mineral contents in sandy, silty and muddy sediments are 15 wt%, 38 wt% and 47 wt%, respectively, and marked as Sandy S, Silty S and Muddy S on the horizontal axis. 200,000 data are displayed here shown as blue dots in figs. A–B and purple dots in figs. C—F. The colored dots in figs. C—F are samples with specific mineral ratios (e.g., red dots in fig. C represent samples with Pl/Kfs ratio of 1), and the colored lines are fitted according to the corresponding samples. CIA and CIX values vary monotonically with grain size, while CIW, PIA, SiO_2/Al_2O_3 and WIP values show non-monotonic variations with grain size due to effects from Pl/Kfs, Qtz/Fsp and Kao/Ill ratios. (For interpretation of the references to colour in this figure legend, the reader is referred to the web version of this article.)

4.2. Distinctive effects of clay mineral species on multi-elemental geochemical indices

Kaolinite, illite, smectite and chlorite are widely distributed in various sedimentary environments throughout the Earth and are the major clay mineral species in sediments (Warr, 2022). Kaolinite and illite are considered as representative products in chemical weathering-dominant and physical weathering-dominant sediments, respectively (Galán, 2006; Fagel, 2007; Chaudhri and Singh, 2012). Diverse source rock lithology of kaolinite and illite and their high abundance in sediments make the kaolinite/illite ratio (Kao/Ill) a popular clay mineralogical proxy for evaluating chemical weathering intensity (Mei et al., 2021; Chen et al., 2023). In the case of rapid physical erosion (short residence time) coupled with strong chemical alteration, the kaolinite/illite ratios in sediments may not solely and accurately characterize chemical weathering intensity (e.g., Borneo and Taiwan river sediments, Huang et al., 2021; Nayak et al., 2021). Smectite is usually produced by moderate chemical alteration of mafic rocks and develops in poor drainage conditions (Keller, 1970; Borchardt, 1989; Galán, 2006). Thus, the kaolinite/smectite ratio (Kao/Sme) is suitable for evaluating strong to moderate chemical weathering without considering the special basaltic lithological setting (e.g., Luzon river sediments, Liu et al., 2012).

Our simulation test results reveal that the proportion of kaolinite and illite has certain influences on all potassium-related indices. Changes of Kao/Ill ratio (0–20) lead to variation range of up to 10 in CIA, PIA, CIX and WIP values under the condition of moderate clay mineral content (CMC = 50 wt%) (Fig. 3, Fig. A4). K/Al and Na/K ratios have remarkable responses to variation in Kao/Ill ratio (Fig. A5), whereas the CIW, SiO_2/Al_2O_3 and Na/Al values have no responses (Fig. A4–A5). Change of kaolinite/smectite ratio (Kao/Sme = 0–20) results in variation range of 5–10 in CIA, PIA and CIX values when the clay mineral content is 50 wt % (Fig. 3, Fig. A4). Surprisingly, SiO_2/Al_2O_3 values fluctuate greatly (ca. 10) with Kao/Sme ratio (Fig. 3). While, Kao/Sme ratio has slight influences on Na/Al, Na/K, K/Al, CIW and WIP values (Fig. A4–A5). Hence, these proxies are not recommended for evaluation of moderate-strong chemical weathering intensity. Chlorite is produced in physical weathering-dominant arid-cold environment (weak chemical weathering) and altered from intermediate and mafic crystalline rocks (Chaudhri and Singh, 2012). The chlorite-involved simulation test results show that the chlorite variables (e.g., kaolinite/chlorite) in sediment clay mineral assemblage significantly affects Fe—Mg elements-related proxies, i.e., the mafic index of alteration (MIA, Babechuk et al., 2014) and α^{Al}_{Mg} (Garzanti et al., 2013b) (Fig. A6). Overall, the influence degree of clay mineral species on chemical weathering indices is closely related to the total clay mineral content in sediments and can be negligible in clay mineral-poor sediments (e.g., the CMC = 10 wt% simulation results; Fig. 3).

The differential effects of clay mineral species on chemical weathering indices can be explained by the distinctive weathering index values assigned to four clay minerals (Fig. A7). Note that the weathering indices values of clay mineral species do not follow the weathering intensity-controlled sequence of chlorite-illite/smectite-kaolinite (Table 1, Fig. A7; Deepthy and Balakrishnan, 2005). Previous case studies suggest that chemical weathering indices may be sensitive only to specific clay mineral proportions and have varying degrees of responses (Fedo et al., 1995; Mir et al., 2016; Sebastian et al., 2019; Zhang et al., 2023). This phenomenon well explains the decoupled results of

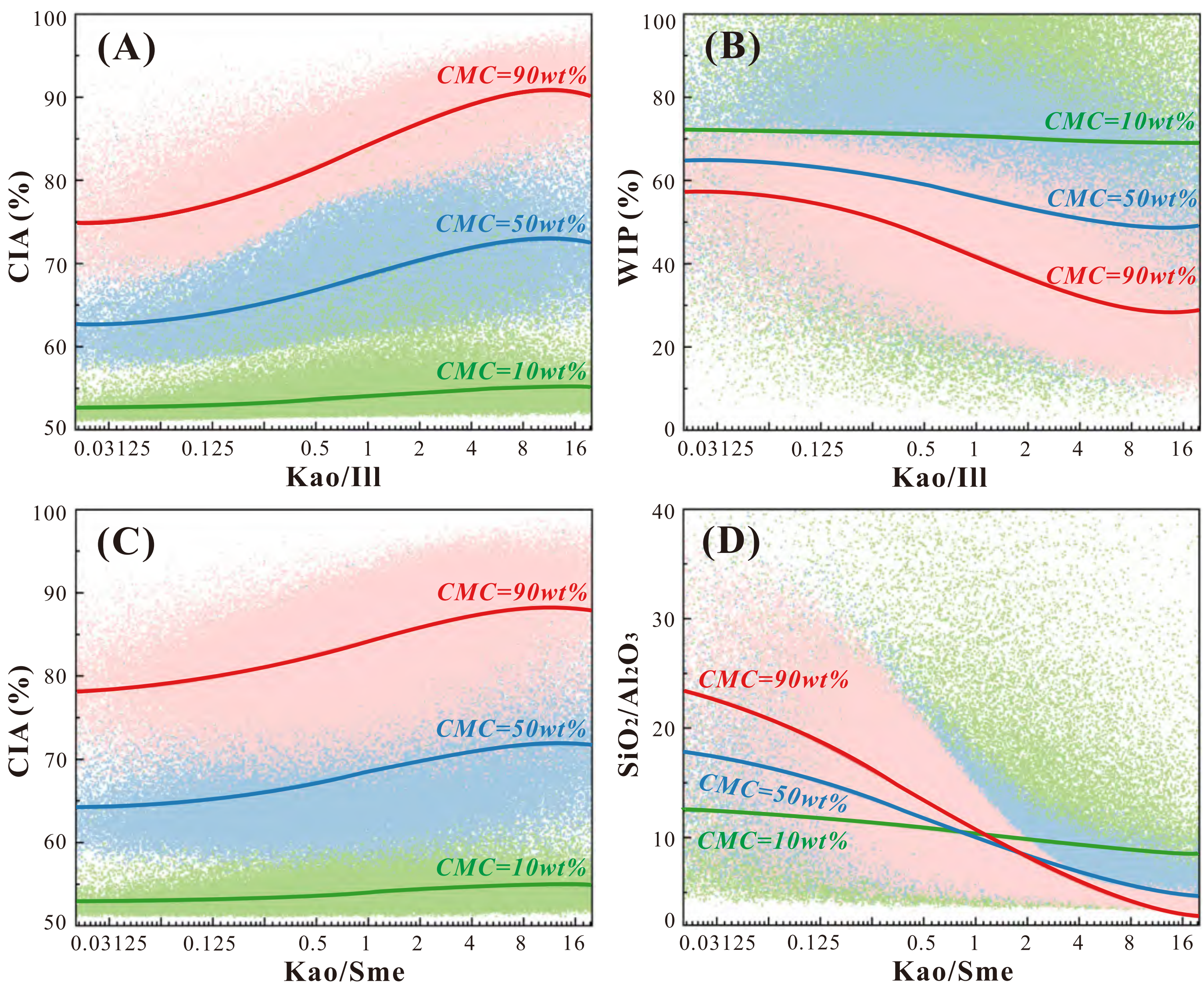

Fig. 3. Responses of CIA, WIP and SiO_2/Al_2O_3 values to changes of clay mineral species (Kao/Ill, Kao/Sme ratios) under different clay mineral content conditions (Clay mineral content is abbreviated as CMC in all figs. CMC = 10 wt%: green, 50 wt%: blue, 90 wt%: pink). Each batch contains 100,000 pieces of data, and three batches of data may overlap. The green, blue and red lines are fitted based on each batch of data. (For interpretation of the references to colour in this figure legend, the reader is referred to the web version of this article.)

clay mineralogical and geochemical proxies in reconstructions of paleo-chemical weathering intensity in some cases. For example, chlorite-rich sediments tend to have high CIA, CIW, PIA and CIX values, resulting in overestimation and misinterpretation of chemical weathering intensity (Nesbitt and Young, 1997; Scheffler et al., 2006; Minyuk et al., 2014; Xu et al., 2017).

4.3. Sensitivity differentiation of CIA, CIW and PIA to feldspar species

Although the CIA, CIW, PIA and CIX indices are regarded as analogous proxies and are corporately used in many case studies (e.g., Buggle et al., 2011; Cao et al., 2019; Perri, 2020; Chen et al., 2021; Sun et al., 2022a). However, these proxies demonstrate diverse responses to variations in plagioclase and K-feldspar proportions (Pl/Kfs ratio = 0–20). Our simulation results show that CIW and PIA values closely depend on Pl/Kfs ratio with the variation ranges of ca. 25–30 at moderate clay mineral content (CMC = 50 wt%) (Fig. 4). CIX values vary with Pl/Kfs ratio in a range of ca. 0–12 (Fig. A8), whereas CIA is almost not affected by Pl/Kfs ratio (Fig. 4). Pl/Kfs ratio affects chemical weathering indices mainly by controlling the proportion of elements Ca, Na and K, for example, increase of Pl/Kfs ratio enhances Ca and Na contents and reduces K content. The CIA proxy can well balance the opposite effects from change of feldspar-bound element concentrations and is the least affected. In the case of reduced Pl/Kfs ratio, CIW, PIA, WIP and K/Al values (Fig. 4, Fig. A8) increase and CIX, Na/K and Na/Al values decrease (Fig. A8), because these weathering indices can't balance the opposite value changes caused by the increase of element K content and decrease of elements Ca—Na content. Results show that CIW, PIA, K/Al, Na/Al and Na/K are extremely sensitive to changes in Pl/Kfs ratios, especially in low clay mineral content conditions (Fig. 4, Fig. A8), whereas changes of Pl/Kfs ratios have minor effect on SiO_2/Al_2O_3 values (Fig. A8).

It is well-known that plagioclase is preferentially weathered than K-feldspar (White et al., 1996). Plagioclase and K-feldspar proportions in sediments are attributed to both chemical weathering intensity and the original mineral compositions of source rocks. For example, Pl/Kfs ratios in mafic rocks (e.g., basalt and gabbro) are higher than that in felsic rocks (e.g., granite and granodiorite) (Nesbitt et al., 1996; Liu et al., 2016a; Sun et al., 2022c). CIW values are expected to be high in K-feldspar-rich sediments/siliciclastic rocks (Fedo et al., 1995), independent of weathering intensity. Thus, CIA is applicable to a wider range of source rock lithology than CIW for evaluation of sediment chemical weathering intensity.

4.4. Significant influence of quartz/feldspar ratio on most weathering indices

The fluctuation of quartz/feldspar ratios (Qtz/Fsp = 0–20) results in value variations in most chemical weathering indices (except for Na/K index), implicating dual-controls of quartz and feldspar content.

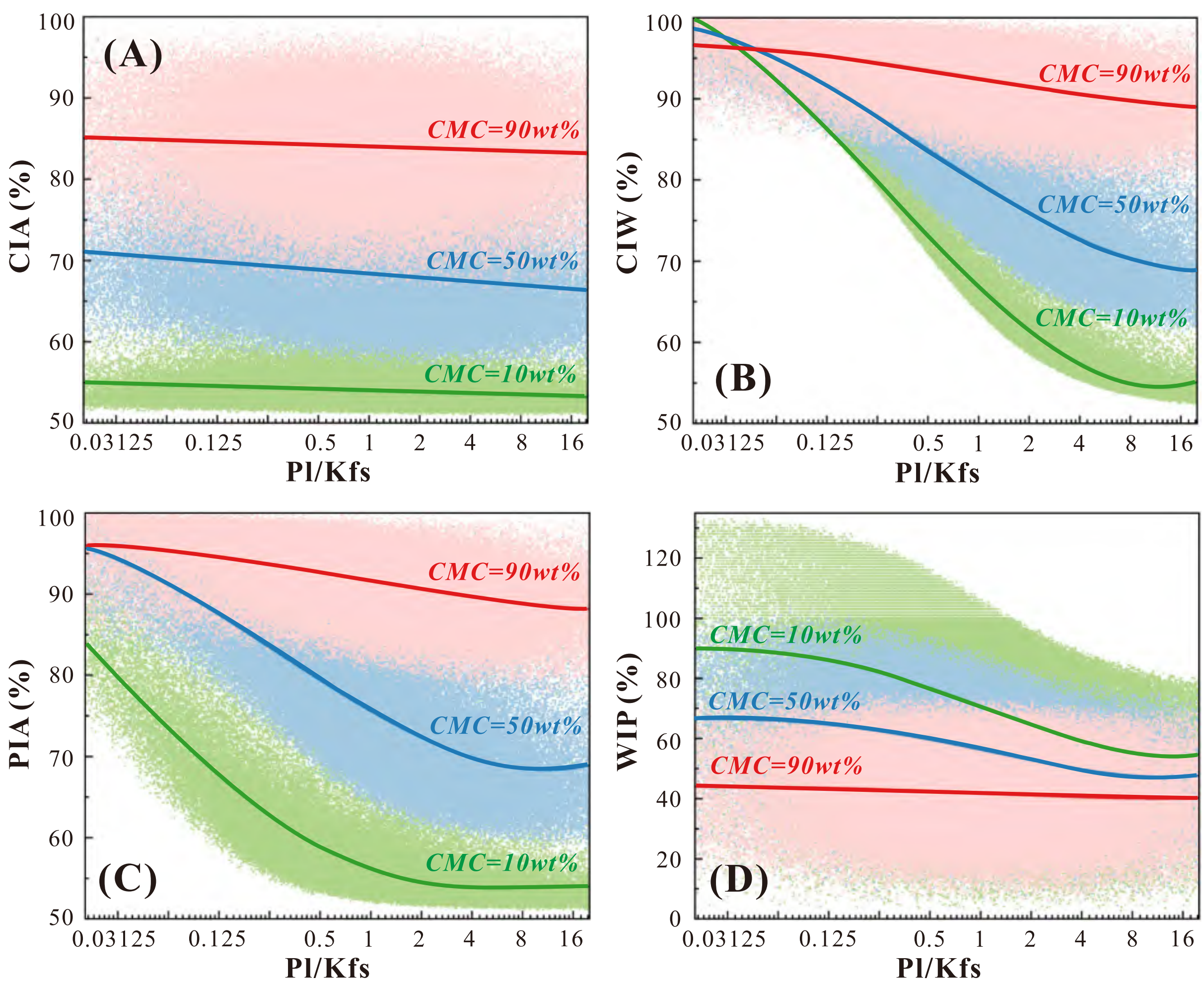

Fig. 4. Responses of CIA, CIW, PIA and WIP values to change of feldspar species (Pl/Kfs ratio) under clay mineral content conditions of 10 wt% (green), 50 wt% (blue) and 90 wt% (pink). Clay mineral content is abbreviated as CMC in the figure. Three batches of data may overlap (100,000 data each batch), and the green, blue and red lines are fitted based on each batch of data. (For interpretation of the references to colour in this figure legend, the reader is referred to the web version of this article.)

Chemical weathering indices CIA, CIW, PIA, CIX, K/Al and Na/Al involve the relative content of elements K, Ca, Na, Al and are thus sensitive to the control of feldspar content. The increase of Qtz/Fsp ratio from 0 to 20 contribute to a range of 15–30 increases in CIA, CIW, PIA and CIX values under moderate clay mineral content (CMC = 50 wt%) conditions (Fig. 5, Fig. A9). K/Al and Na/Al values vary moderately with the Qtz/Fsp ratios (Fig. A9). The substantial reduction of WIP value (e.g., 55 at CMC = 50%) with increase of Qtz/Fsp ratio is closely related to quartz dilution effect, especially in recycled, compositionally-mature sediments (Fig. 5; Garzanti et al., 2013a). We note that WIP was defined to measure the absolute concentration of easily-mobile elements (i.e., K, Ca, Na, Mg) in sediments, which essentially depends on the absolute concentrations of feldspar and quartz. The SiO_2/Al_2O_3 ratio of clay-poor sediments (CMC = 10 wt%) is remarkably influenced by quartz and feldspar contents and indicates a clear positive correlation with Qtz/Fsp ratio (Fig. 5).

Due to the different response intensity of CIA and WIP to the absolute content of quartz, CIA-WIP plot is widely applied to discriminate first-cycle sediment weathering and sedimentary recycling (Garzanti et al., 2014; Schneider et al., 2016; Dinis et al., 2017; Guo et al., 2017, 2018; Xie et al., 2018; Wang et al., 2019b). The SiO_2/Al_2O_3 index is commonly used to characterize sediment grain size, and the relationship between CIA and SiO_2/Al_2O_3 is proposed as an important criterion to determine the grain size effect on sediment chemical weathering intensity evaluation (Guo et al., 2018). However, we suggest that the SiO_2/Al_2O_3 value mainly depends on sediment mineral compositions rather than grain size distributions, for example, high sensitivity to changes of quartz content (Qtz/Fsp ratio, Fig. 5) and clay mineral species (Kao/Sme ratio, Fig. 3). Our simulation test results indicate that the SiO_2/Al_2O_3 value as a reliable proxy of hydrodynamic sorting (or sediment grain size) only applies to sediments with high Qtz/Fsp and Kao/Sme ratios (Fig. 3, Fig. 5). Theoretically, the Qtz/Fsp and Kao/Sme ratios in sediments may depend on several processes, such as chemical weathering, supply of source materials, hydrodynamic sorting sedimentary recycling and diagenetic transformation (Nesbitt et al., 1996; Carriquiry et al., 2001; Mikesell et al., 2004; Caracciolo et al., 2012; Garzanti, 2019; Stone et al., 2019). Additionally, the presence of biological silica, especially that in marine sediments, may affect SiO_2/Al_2O_3 ratio (Varela et al., 2004). In this case, pretreatment is required to remove biological silica prior to evaluation of chemical weathering intensity.

4.5. Summary

The Pearson's correlation coefficient (r) is calculated and employed to quantitively reveal the correlation and response intensity between chemical weathering indices and mineral compositions (Fig. 6; Table A3). The closer $|r|$ value is to 1, the higher Pearson correlation and the stronger influence of mineral composition on weathering indices. A negative r-value indicates a negative correlation between weathering index values and mineral proportions, and vice versa. The total clay mineral content in sediments is the primary control on majority of multi-elemental weathering indices ($|r| > 0.5$) except for SiO_2/Al_2O_3 and Na/K (Fig. 2, Fig. 6). Clay mineral species have differentiated (most $|r| <$ 0.4, Fig. 6) and noteworthy effects on weathering indices for clay

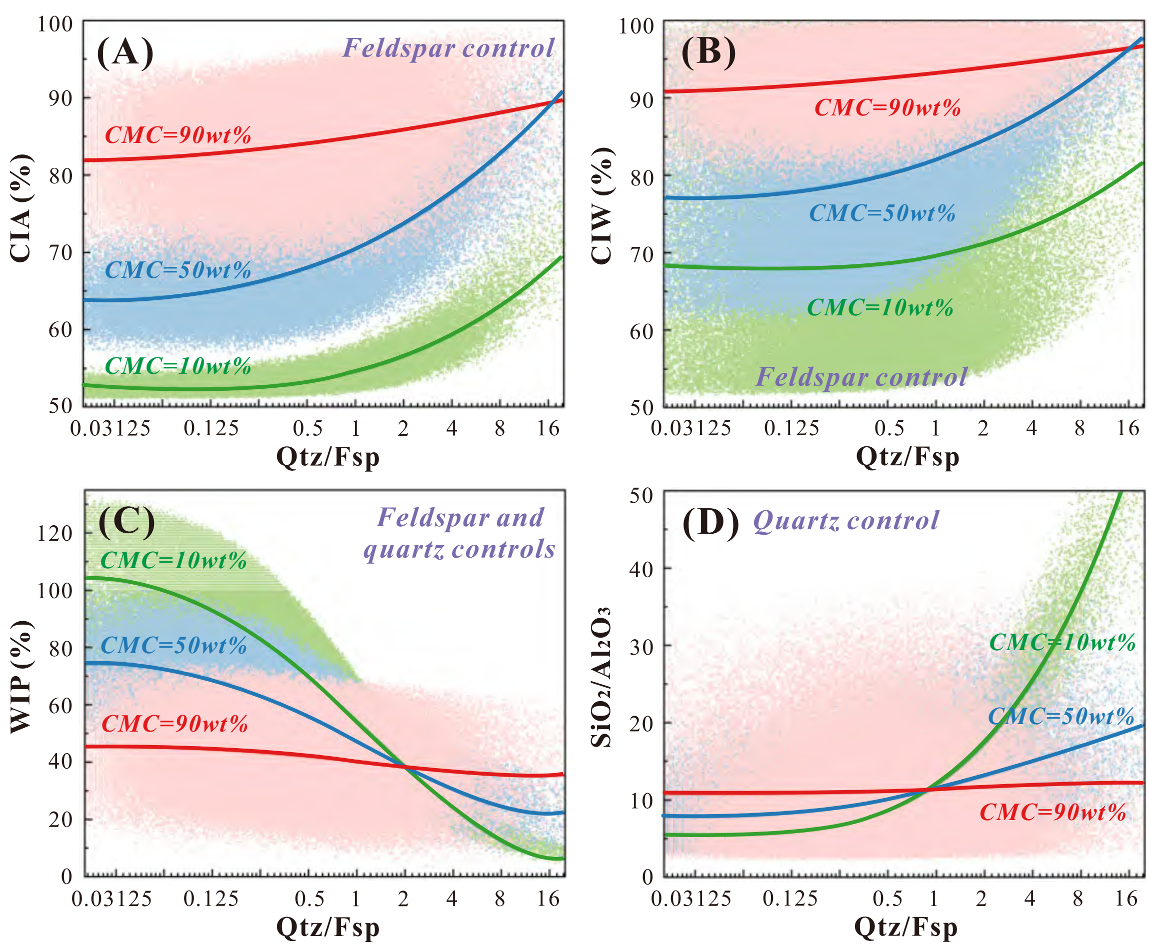

Fig. 5. Responses of CIA, CIW, WIP and SiO_2/Al_2O_3 values to change of Qtz/Fsp ratio under clay mineral content conditions of 10 wt% (green), 50 wt% (blue) and 90 wt% (pink). Clay mineral content is abbreviated as CMC in the figure. Three batches of data may overlap, and the green, blue and red lines are fitted based on each batch of data. CIA and CIW are mainly affected by feldspar content and SiO_2/Al_2O_3 is controlled by quartz content, whereas WIP are both controlled by feldspar and quartz content. (For interpretation of the references to colour in this figure legend, the reader is referred to the web version of this article.)

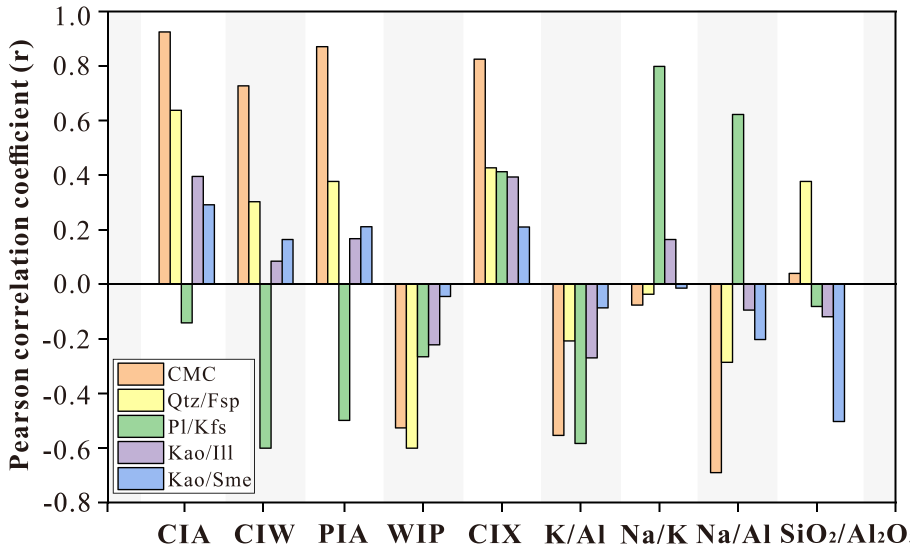

Fig. 6. Sensitivity differences of weathering indices to changes in mineral proportions (clay mineral content, quartz/feldspar, plagioclase/K-feldspar, kaolinite/illite, and kaolinite/smectite ratios). Clay mineral content is abbreviated as CMC. All the simulated data are employed here. Pearson's correlation coefficient (r) (with significance levels at $p < 0.01$) performed with SPSS suite is used to illustrate the correlation and response intensity between weathering indices and mineral ratios. The closer r value is to 1 or − 1, the higher Pearson correlation, indicating the stronger influence of mineral composition on weathering indices. Negative values of Pearson's correlation coefficient mean that the weathering index value has negative correlation with the mineral proportion, and vice versa.

mineral-rich sediments. Inspiritingly, Kao/Sme ratio takes significant control of SiO_2/Al_2O_3 value ($r = -0.5$) and Kao/Ill ratio has prominent influence on CIA and CIX indices ($r = 0.4$, Fig. 3, Fig. 6, Fig. A4). As for detrital minerals (Qtz/Fsp ratio), feldspar content has extensive and intense effects on CIA, CIW, PIA, WIP and CIX indices and quartz content largely dominates SiO_2/Al_2O_3 (r = 0.4) and WIP values ($r = -0.6$) (Fig. 5, Fig. 6, Fig. A9). Feldspar species (Pl/Kfs ratio) has significant influence on CIW, PIA, K/Al, Na/Al and Na/K indices values ($|r| > 0.5$, Fig. 4, Fig. 6, Fig. A8). However, CIA and SiO_2/Al_2O_3 is least affected by the feldspar species (Fig. 4, Fig. 6, Fig. A8).

5. Factors in sediment source-to-sink processes control mineral compositions, grain size and weathering intensity evaluation

Sediment source-to-sink systems involve a series of geological processes (Fig. 1). Except for chemical weathering, sediment mineral compositions are also related to source rock materials, erosion rate, hydrodynamic sorting, biological effect, deposition and diagenesis conditions (Prudêncio et al., 2002; Singh, 2009; Su et al., 2015; Molina et al., 2019). These processes or factors result in bias in sediment chemical weathering intensity evaluation. Here, we mainly focus on five influential factors and processes including source rock lithology (e.g., felsic and mafic igneous rocks; sedimentary recycling) (Cox et al., 1995; Nesbitt et al., 1996), climatic condition (Nesbitt and Young, 1982), physical erosion (Riebe et al., 2001), hydrodynamic sorting (Shao and Yang, 2012) and diagenesis (Fedo et al., 1995).

5.1. Source rock lithology

Sediment compositions partially inherit mineral assemblages of source materials. Source rock lithology has been considered as an interference in chemical weathering intensity evaluation (Garzanti and Resentini, 2016; Guo et al., 2018; Chen et al., 2021). The felsic-intermediate-mafic crystalline rocks contain distinctive plagioclase, K-feldspar and quartz contents. For example, the Pl/Kfs ratio and Qtz/Fsp ratio of granite are ca. 1.5 and 0.5–1, while those of gabbro are ca. 49 and 0, respectively (Nesbitt and Young, 1984; Lee et al., 2008; Tavakoli et al., 2020). Clay mineral compositions in sediments are also related to source rock lithology. Smectite and chlorite are preferentially produced from volcanic or mafic rocks which contain Fe-, Mg-rich minerals, whereas illite and kaolinite tend to be formed in weathered granitic terranes (Locsey et al., 2012; Zhang et al., 2021b).

To simulate sediments from lithologically-diverse source rocks, we collect mineralogical data of top-layer weathered materials from in-situ weathering profiles developed on mafic-, felsic- crystalline rocks and quartz-rich riverine sediments/sandstones (representing a sedimentary recycling endmember) across climatic zones (Nesbitt et al., 1996; Le Pera and Sorriso-Valvo, 2000; Ma et al., 2007; Lee et al., 2008; Raza et al., 2010; Etemad-Saeed et al., 2011; Locsey et al., 2012; Yusoff et al., 2013; Su et al., 2015; Liu et al., 2016a; Garzanti et al., 2018, 2019; Gong et al., 2019; Chen et al., 2020b; Cruz et al., 2021; Mei et al., 2021). Three source rock endmembers are set in the simulation test, i.e., granite, basalt and quartzose sandstones. Although some case studies have shown the mismatch between climate and chemical weathering intensity, e.g., subtropical Taiwan and Fujian provinces in China (Selvaraj and Chen, 2006; Su et al., 2015; Guo et al., 2018). We suppose that sediments produced under the same climatic condition with similar background of source rock lithology, physical erosion rate and landform experience consistent intensity of chemical weathering. The original mineral data used in our "lithology effect" simulation mainly refer to the highly-weathered materials from in-situ weathering profiles, which may avoid interferences of source rock lithology and tectonic setting and minimize the possibility of irrelevant climate and weathering degrees. Based on the collected climatic data from above-mentioned case studies, we roughly classify four levels of chemical weathering intensity, namely strong, moderate, mild and weak, correlating with climatic conditions of tropical, subtropical, temperate and frigid zones, respectively (Table A5). The simulated parameters including specific sediment compositions and source mixing patterns are shown in Table A4–A6 and Fig. 7.

Here, we mainly focus on the WIP and CIA indices. The simulation results indicate that lithology bias dramatically change WIP values (variation range of 72) in clay-poor sediments under weak weathering conditions (Fig. 7B). Actually, the large shift of the WIP values is controlled by feldspar content in sediments (Table 4, Fig. A10), and the variation range is consistent with the response (55–100 at CMC < 50 wt %, Fig. 5) of WIP to changes of Qtz/Fsp ratios. The variations in the relative content of clay minerals and feldspar in sediments ($R^2 > 0.98$, Fig. A10) result in a range of 28 shift for the CIA values under moderate weathering conditions (Fig. 7B). This phenomenon is a confirmation of

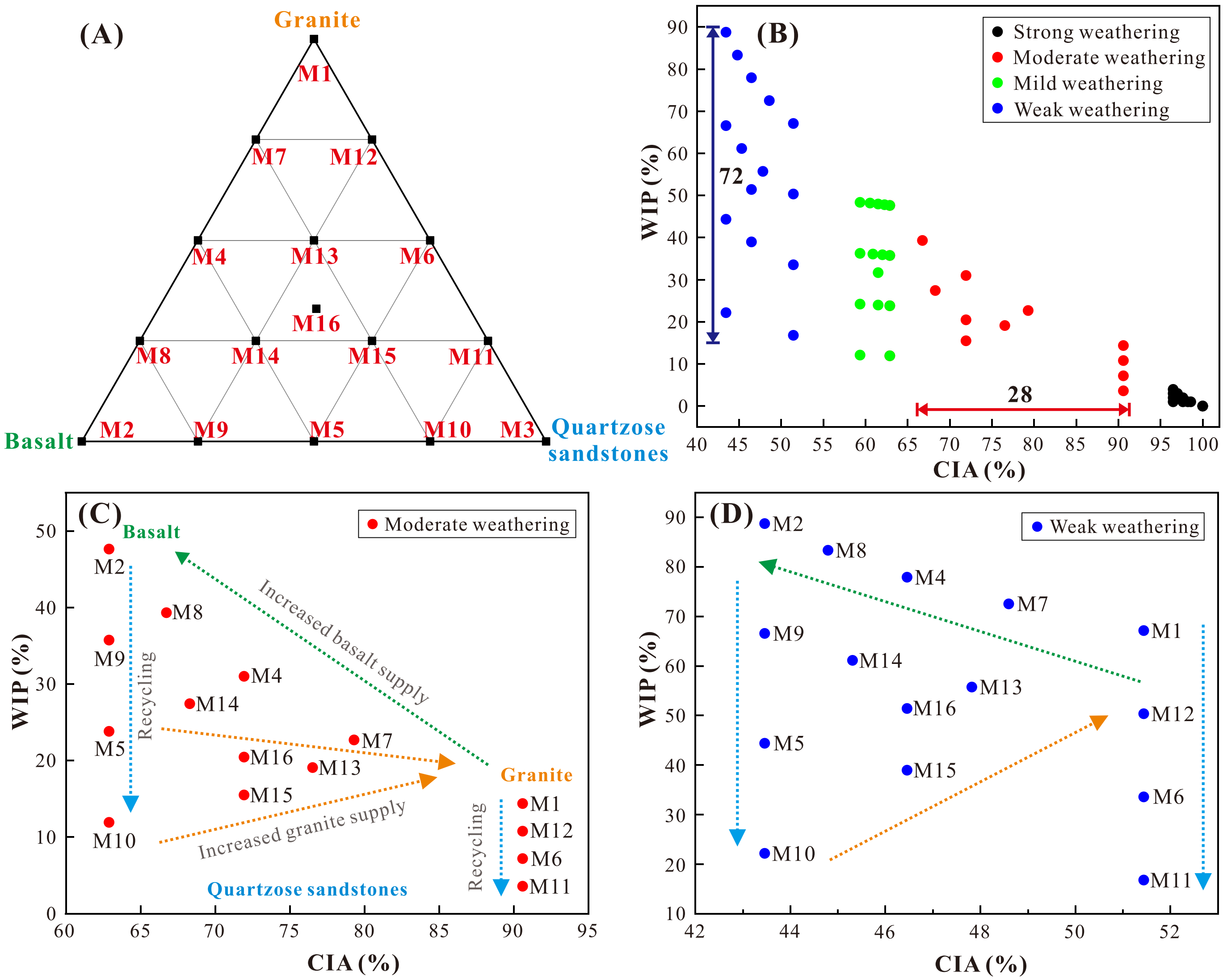

Fig. 7. (A) 16 types of simulated sediments (labeled M1–M16) mixed proportionally from three endmembers of materials derived from granite, basalt and quartzose sandstone. For example, samples M1, M2, M3 are 100% supplied from granite, basalt and quartzose sandstone, respectively. Sample M7 is composed of 75% granite- and 25% basalt-sourced materials. Specific mixed patterns of simulated sediments are shown in Table A6. (B) Comparison of WIP and CIA values in sediments with mixed lithologies (16 types) under different chemical weathering conditions. (C) The similar distribution patterns of CIA-WIP plots responding to source lithology effect in moderate weathering and (D) weak weathering conditions. Figs. C and D are zoom-in versions of the relevant content in Fig. B.

the numerical simulation results (CMC = 50 wt%, Qtz/Fsp, CIA range of 27, Fig. 5). It is further proved that even under moderate-strong weathering conditions, source signals can retain in sediment compositions and thus affect weathering intensity evaluation (related studies, e.g., Peketi et al., 2020; He et al., 2020; Garzanti et al., 2021). Increase of basalt-sourced materials results in decrease of CIA and increase of WIP values (green arrow, Fig. 7C). Except for feldspar, Fe, Mg-rich minerals (pyroxene and olivine) in mafic rocks may have minor effects on CIA and WIP values (Table 1). WIP is strongly coupled with sedimentary recycling, indicating quartz dilution effect. The reduction amplitude of WIP values with recycling is closely related to the felsic- and mafic-rock proportions mixed in source rock endmembers (blue arrow, Fig. 7). The response patterns of CIA and WIP values to sediments with changeable source rock lithologies are similar under moderate and weak weathering conditions (Fig. 7), indicating that lithology bias may be independent of weathering intensity and climatic conditions. Therefore, we suggest that lithology bias is prevailing in chemical weathering studies, especially for modern basin sediments and deep-time sedimentary rocks with diverse or changeable sources.

5.2. Climate and physical erosion

Different climate conditions highly impact detrital plagioclase, K-feldspar and quartz contents (Kamp, 2010) and the clay mineral species (Biscaye, 1965; Rateev et al., 1969; Fagel, 2007; Varga et al., 2011; Dill, 2020) in sediments. According to the numerical simulation results, CIA values increase in a range of 40 with the co-changes of clay mineral content (Fig. 2), Qtz/Fsp ratio (Fig. 5) and Kao/Ill ratio (Fig. 3). The change amplitude of CIA values for the simulated sediments is consistent with variation of CIA values in weathered materials developed on granite weathering profiles at different latitudes in China (from temperate climate to tropical climate, Mao et al., 2022).

Chemical weathering process is commonly divided into supply-limited and kinetic-limited regimes (West et al., 2005; Chen et al., 2020c). Supply-limited weathering happens in weakly-eroded regions with limited weatherable substances, controlled by the supply rate of fresh materials, i.e., weathering rate and intensity are dominated by physical erosion (Riebe et al., 2001; Larsen et al., 2014). However, the enhanced physical erosion rate may shorten the residence time of weatherable materials, resulting in insufficient weathering of primary minerals (Dixon et al., 2012). Therefore, the excessive physical erosion rate (e.g., > 10^2 t km^{-2} yr^{-1}) may shift the weathering regime from supply-limited to kinetic-limited and inhibit chemical weathering (Gabet and Mudd, 2009). Kinetic-limited weathering develops in strongly-eroded regions with sufficient fresh materials, controlled by the kinetic dissolution rate of minerals, i.e., weathering rate and intensity are dominated by climatic condition (Ferrier et al., 2016; Riebe et al., 2017; Fu et al., 2022; Mao et al., 2022).

In the supply-limited weathering regime, increase of physical erosion rate does not significantly change sediment compositions due to available temperature and precipitation conditions. However, in the kinetic-limited weathering regime, sediment compositions are characterized by more source material inheritance and less chemical alteration (Hren et al., 2007; Emberson et al., 2016; Guo et al., 2018; Fu et al., 2022). For example, fluvial sediments in highly-eroded Taiwan contain fresh detrital feldspars and major amounts of mild-weathering products (i.e., chlorite and illite) with low CIA values of 48–75 (Liu et al., 2012; Garzanti and Resentini, 2016). The alteration of sediment compositions by physical erosion due to changes of tectonic activity, geomorphic factors and precipitation intensity has been regarded as the prevailing bias in the paleoclimate reconstruction via analyzing paleo-chemical weathering intensity (Varga et al., 2011; Jian et al., 2019; Fu et al., 2022).

5.3. Sediment transport and depositional dynamics

In sediment transport and deposition processes, hydrodynamic condition plays an important role in deciding the motion state of detrital materials (transport or deposition). Change of hydrodynamic intensity causes sedimentary sorting due to grain size, particle shape and density differences of particles, thusly modifies mineralogical and further chemical compositions of sediments (Lupker et al., 2013; Zhang et al., 2021a). Coarse-grained sediments (e.g., sand fractions) contain abundant quartz, feldspar and relatively small amounts of clay minerals. By contrast, fine-grained sediments (clay-silt fractions) are rich in phyllosilicates such as micas and clay minerals. In elemental chemistry perspectives, it is generally believed that coarse-grained sediments contain relatively high Si, Na, Ca and low Al concentrations than fine-grained sediments (Lupker et al., 2013; Cao et al., 2017; Chen et al., 2021). There are exceptions that illite-rich muddy sediments (100 wt% illite: SiO_2/Al_2O_3 = 5.4) may produce higher SiO_2/Al_2O_3 values than plagioclase-rich sandy sediments (100 wt% plagioclase: SiO_2/Al_2O_3 = 3.3) based on the theoretical calculation.

Grain size bias in chemical weathering intensity evaluation has been well discussed (e.g., Shao et al., 2012; Jian et al., 2013; Chen et al., 2021; Chen et al., 2022). Previous studies reported that multi-elemental indices (i.e., CIA, CIW, PIA, WIP, CIX) values differ by up to 15 in the analysis of coarse-grained (e.g., sand) and fine-grained (e.g., silt and mud) sediments (Chen et al., 2021; Zhang et al., 2021a). Our simulation results show that the increases in CIA and CIX values from simulated sandy to muddy sediments are ca. 15 (Fig. 2). Changes in feldspar species and content induced by grain size effect cause the largest variation range of 20 in CIW, PIA and WIP values between sandy and muddy sediments (Fig. 2). We also note that the four clay minerals have different particle size and swelling capacity (Gibbs, 1977; Bengtsson and Stevens, 1998; Tan et al., 2017). This grain-size dependency of clay mineral distribution is worthy to be explored when considering the hydrodynamic sorting bias.

Investigators attempted to (1) propose an A-CNK-Si diagram (Guo et al., 2021), (2) evaluate the correlation between CIA and grain size proxies, e.g., Al/Si, Ti/Al, Zr/Rb and Zr/Al_2O_3 (Liang et al., 2013; Pang et al., 2018; Greber and Dauphas, 2019), (3) extract sediment fractions with specific grain size for weathering evaluation (Ren et al., 2019), and (4) calibrate CIA value based on Al/Si ratio (Li et al., 2022a; Li et al., 2022b) to distinguish (the above 1–2) or reduce (the above 3–4) grain size bias on sediment chemical weathering intensity evaluation. The SiO_2/Al_2O_3 ratio is widely used as a sediment grain size proxy to address the influence of hydrodynamic sorting because SiO_2 is mainly hosted in quartz and feldspar in coarse-grained fractions and Al_2O_3 is concentrated in phyllosilicates in fine-grained fractions (Chen et al., 2021; Zhang et al., 2021a). However, we suggest that using Al/Si ratio to correct CIA values should notice the influences from other mineral proportions (Fig. 6), e.g., changes of quartz content (Qtz/Fsp ratio, Fig. 5) and clay mineral species (Kao/Sme, Fig. 3). Our simulation results by modeling sediments generated in moderate weathered granitic drainage terranes (Table A7) show that the quantitative data of corrected CIA values are ambiguous because of the subjective selection of standardized parameters ($(Al/Si)_N$, Fig. A11). Additionally, the qualitative trends of corrected CIA values probably erase chemical weathering signals contained in elements Al and Si independent of grain size. Eliminating sediment grain size bias in chemical weathering intensity evaluation is still a challenge and deserves further study.

5.4. Diagenetic K-metasomatism

Paleo-chemical weathering intensity reconstruction based on deep-time sedimentary records may experience diagenetic bias. During the formation of sedimentary rocks, post-depositional diagenesis can alter the mineralogical and chemical compositions. K-metasomatism-related illitization receives a lot of attention in chemical weathering studies, especially for fine-grained sedimentary rocks (Yang et al., 2016; Xu et al., 2017; Dai et al., 2022; Sun et al., 2022b). The A (Al_2O_3)-CN (CaO + Na_2O)-K (K_2O) ternary diagram has been widely employed to recognize diagenetic K-metasomatism. Element geochemical data of weathered sediments plotted in the A-CN-K diagram are expected to follow an ideal weathering trend based on thermodynamic and kinetic calculations, first parallel to the A-CN boundary and turning towards the A apex as it approaches the A-K boundary (Nesbitt and Young, 1982). Plotted data deviate from the ideal weathering trend and turn towards the K apex in response to the effect of diagenetic K-metasomatism (e.g., Fedo et al., 1995; Dai et al., 2022; Sun et al., 2022b).

Kaolinite, smectite and K-feldspar are potential precursors for illitization. Smectite illitization has a wide temperature range (30–100 °C, 70–250 °C as reported) and the most proper condition is 50–60 °C with a burial depth of 3 km (Cuadros, 2006; Li et al., 2019b; Dowey and Taylor, 2020; Ali et al., 2021). Kaolinite illitization occurs in the late diagenesis stage at temperatures above 125 °C and depths of ca. 3.5–4 km, requiring moderate concentration of K^+/H^+ ions (Berger et al., 1997; Lanson et al., 2002; Li et al., 2019b; Wang et al., 2019a). K-feldspar illitization tends to form in the acidic fluid environments (Wang et al., 2019a). Observations from (1) the increased proportion of illite with section depth (Liang et al., 2021), (2) the morphology of clay minerals by the scanning electron microscope (Xu et al., 2017), (3) the maturity of organic matter (Dellisanti et al., 2010), and (4) the illite crystallinity index (Kübler index, Jaboyedoff et al., 2001) can help to determine the level of diagenetic illitization.

Kaolinite-illitization utilizing the exogenous potassium from hydrothermal fluids (Lanson et al., 2002) may reduce Kao/Ill ratio, resulting in decrease of CIA, PIA, CIX values and increase of WIP value (Fig. 6). However, Kaolinite-illitization utilizing the endogenous potassium from dissolution of K-feldspar and mica in sediments (Dowey and Taylor, 2020) may decrease Kao/Ill ratio and increase Qtz/Fsp and Pl/Kfs ratios, resulting in contrary and superposed effects on weathering indices. We speculate that the consequence is the increases in CIA and CIX values and decreases in CIW, PIA and WIP values because of their different sensitivity to changes of mineral ratios (Fig. 6). Except for diagenetic K-metasomatism, the effects of other diagenetic transformations of minerals and elements on chemical weathering intensity evaluation have not been systematically evaluated yet and are worthy of further study.

6. Conclusions, implications and perspectives

6.1. Conclusions

We employ the Monte Carlo method to simulate sediments with different mineral compositions to quantitively evaluate the influences of siliciclastic sediment heterogeneity on major element-based weathering indices (i.e., CIA, CIW, PIA, WIP, CIX, K/Al, Na/Al, Na/K and SiO_2/Al_2O_3). We also review the influences of external factors in sediment source-to-sink processes (source rock lithology, climate, physical erosion, hydrodynamic sorting and diagenetic K-metasomatism) on application of chemical weathering indices, and yield the following conclusions:

(1) Total clay mineral content in sediments, dominated by hydrodynamic sorting and source chemical weathering, is the primary control on most chemical weathering indices values, especially for CIA, CIW, PIA and CIX. Clay mineral species (represented by Kao/Ill, Kao/Sme ratios etc.), tightly coupled with sediment source-to-sink processes, have distinctive and noteworthy influences on these weathering indices when analyzing clay mineral-rich sediments.

(2) Feldspar content, which reflects the amount of weatherable substance, has significant impacts on CIA, CIW, PIA, WIP, CIX, K/Al and Na/Al. Majority of chemical weathering indices are insensitive to quartz dilution, except for WIP and SiO_2/Al_2O_3. Feldspar species, i.e., plagioclase and K-feldspar proportions in sediments, have little effect on CIA, moderate effects on WIP and CIX, and remarkable effects on CIW, PIA, K/Al, Na/Al and Na/K values.

(3) Grain size bias and source rock lithology bias on weathering intensity evaluation are highlighted in this study. Grain size bias on weathering indices is essentially achieved by differentiating sediment mineral compositions. Value differences of multi-elemental weathering indices (i.e., CIA, CIW, PIA, WIP and CIX) between sandy and muddy sediments can reach to 20. Weathering materials supplied from different source rock lithologies (felsic-, mafic- crystalline rock and recycled sedimentary rock)

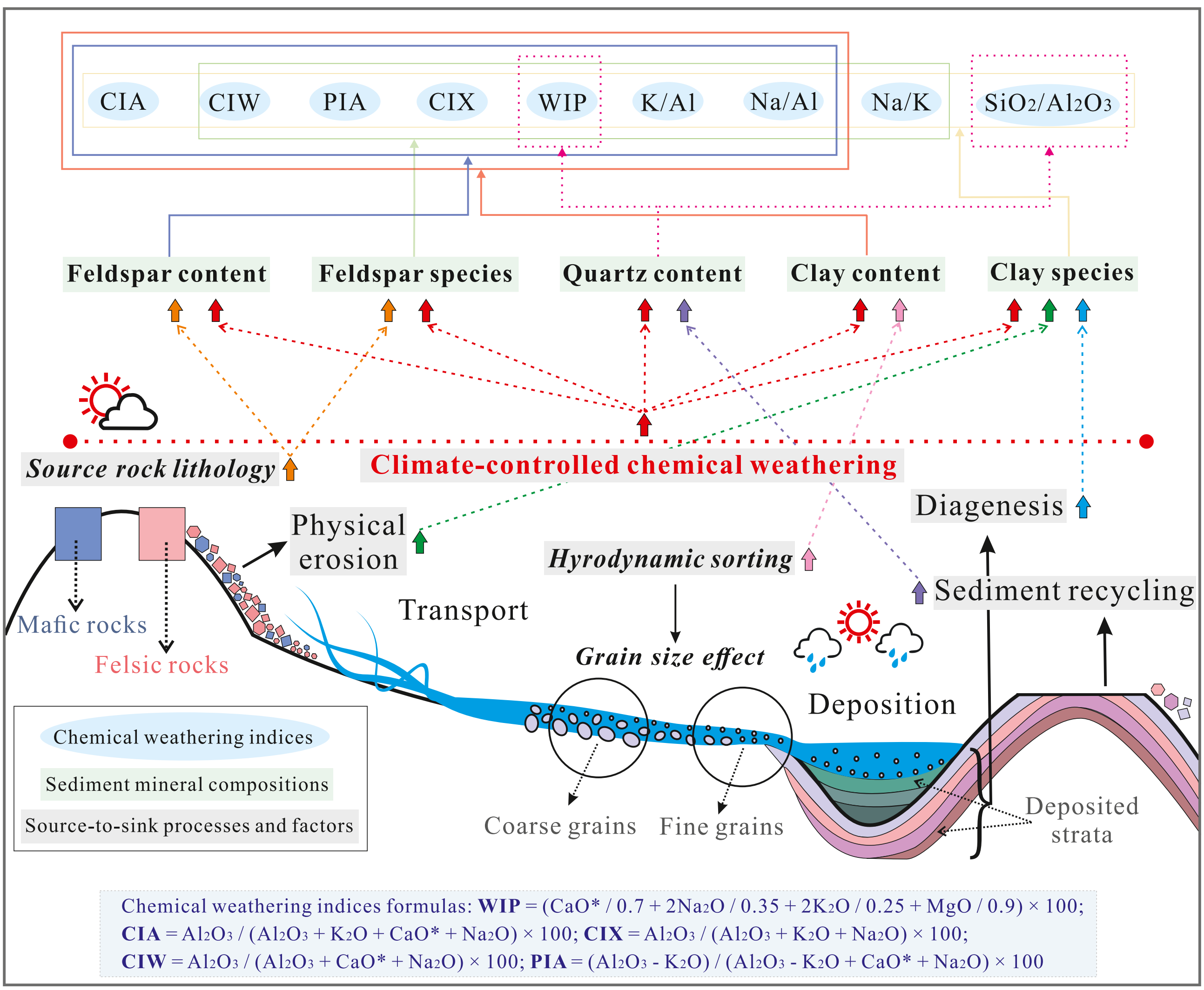

Fig. 8. Schematic diagram of the links among sediment source-to-sink processes, sediment mineral compositions, and chemical weathering indices values. Mineral compositions include quartz content, feldspar content and species, clay mineral content and species. The typical influences of source rock lithology, chemical weathering, physical erosion, hydrodynamic sorting, diagenesis and sediment recycling on mineral compositions are represented in yellow, red, green, pink, blue and purple arrows, respectively. Additionally, the effects of specific mineral compositions (e.g., quartz content) on certain weathering indices (e.g., WIP and SiO_2/Al_2O_3) are marked with colored lines and range boxes (e.g., Magenta). The formulas for chemical weathering indicators are at the bottom of the figure. CaO* represents the CaO associated with silicate component in the sample. (For interpretation of the references to colour in this figure legend, the reader is referred to the web version of this article.)

may significantly change weathering indices values by affecting feldspar fertility and clay mineral species.

6.2. Implications and perspectives

Siliciclastic sediment chemical weathering intensity is widely used as an effective proxy for paleoclimate reconstruction (e.g., Yang et al., 2004; Zhai et al., 2018; Li et al., 2019a; Lv et al., 2022; Li et al., 2022b). However, chemical weathering signals are difficult to be accurately extracted from sediment compositions because of the close integrations of source-to-sink processes and their co-effects on sediments. This study, from the numerical simulation perspective, verifies the mineralogical bias in sediment chemical weathering intensity evaluation. Our findings highlight the interference of source rock lithology (Fig. 7) and hydrodynamic sorting (Fig. 2) on weathering indices. The integrated effects of the external factors or processes in source-to-sink systems on sediment composition and subsequent effects on chemical weathering indices values are shown in a schematic diagram (Fig. 8). These biases may mislead interpretations for paleoclimate and paleoenvironment, thus we suggest improving the accuracy of paleoclimate reconstruction based on paleo-weathering analysis through (1) comprehensive utilization of various chemical weathering indices and (2) systematic analysis of mineralogy, grain size, provenance and even diagenetic evaluation on targeted sediments.

Mineralogical (e.g., Qtz/Fsp, Pl/Kfs, Clay/Fsp, (Kao + Sme)/(Ill+Chl), illite crystalline index, illite chemistry index), major and trace elemental (e.g., mafic index of alteration (MIA), α^{Al}_{Na}, Rb/Sr, Th/K), stable isotopic (e.g., δ^{7}Li, δ^{41}K, δ^{30}Si), and textural (surface textures in mineral grains) weathering indicators have different advantages and disadvantages (McLennan et al., 1995; Kamp, 2010; Andò et al., 2012; Opfergelt and Delmelle, 2012; Garzanti et al., 2013b; Babechuk et al., 2014; Clift et al., 2014; Dellinger et al., 2017; Hossain et al., 2017; Li et al., 2019c; Dinis et al., 2020; Fu et al., 2022), which may produce complementary effects on evaluation of chemical weathering intensity. Previous studies have formed systematic methods to determine external interferences, for example, (1) using the A-CN-K diagram to indicate and calibrate diagenesis K-metasomatism (Fedo et al., 1995; Lin et al., 2020; Chen et al., 2022); (2) applying the La-Th-Sc ternary diagram and Th/Sc ratios to determine changes of provenance (Zhao and Zheng, 2015; Bao et al., 2019; Sun et al., 2022a); (3) using the CIA vs. WIP plot, Th/Sc vs. Zr/Sc plot and compositional variability (ICV) index to evaluate addition of recycled materials (Kafy and Tobia, 2022; Sun et al., 2022a; Zeng et al., 2022); (4) explaining the good correlation of Al_2O_3/SiO_2 and CIA (may not applicable under special circumstances), or the negative correlation of Th and Ti—Zr and the positive correlation of Ca—Na and Ti—Zr to reflect hydrodynamic sorting effect (Zhao and Zheng, 2015; Li et al., 2019c; Sun et al., 2022a; Zeng et al., 2022); (5) extracting and analyzing sediment components within specific grain size ranges (Guo et al., 2017, 2018), and even (6) proposing new weathering proxies $\Delta\varepsilon_{Hf(i)CLAY}$ and Rb/Al for clay-sized fraction of sediments/sedimentary rocks (Bayon et al., 2022). Although some of these methods might be questionable or imperfect, we consider that all the attempts are important and have potentials to be improved in future studies.

Majority of studies on paleo-weathering intensity address local issues and display the diversity of interferences, however, cannot propose universal application laws for identifying and reducing distractions. Looking ahead, detailed and rigorous investigations on modern sediment source-to-sink processes are expected to be beneficial to understand weathering mechanism and are better to reconstruct the past. Numerical simulations and modellings are encouraged and necessary to improve the accuracy of chemical weathering intensity evaluation based on systematic and scientific theory of sediment source-to-sink systems.

CRediT authorship contribution statement

Hanjing Fu: Investigation, Methodology, Validation, Formal analysis, Writing – original draft, Writing – review & editing. **Xing Jian:** Conceptualization, Resources, Project administration, Writing – original draft, Writing – review & editing, Supervision, Funding acquisition. **Hanqing Pan:** Methodology, Validation, Formal analysis.

Declaration of Competing Interest

We declare that we don't have any conflict of interest.

Data availability

The data used in this study have been presented as figures and tables in the manuscript and appendix.

Acknowledgments

This study was supported by the Natural Science Foundation of Xiamen City (No. 3502Z20227006) and the National Natural Science Foundation of China (No. 41806052). We are grateful to the editor and three anonymous reviewers for thoughtful and constructive comments on this manuscript.

Appendix A. Supplementary data

Supplementary data to this article can be found online at https://doi.org/10.1016/j.earscirev.2023.104574.

References

Ali, A., Salman, M., Ahmad, R., 2021. Smectite illitization of the Talhar shale, Lower Goru Formation, Southern Indus Basin, Pakistan. J. Pet. Explor. Prod. Technol. 11 (6), 2315–2325. https://doi.org/10.1007/s13202-021-01183-5.

Andò, S., Garzanti, E., Padoan, M., Limonta, M., 2012. Corrosion of heavy minerals during weathering and diagenesis: a catalog for optical analysis. Sediment. Geol. 280, 165–178. https://doi.org/10.1016/j.sedgeo.2012.03.023.

Arnscheidt, C.W., Rothman, D.H., 2022. Presence or absence of stabilizing Earth system feedbacks on different time scales. Sci. Adv. 8 (46), eadc9241 https://doi.org/10.1126/sciadv.adc9241.

Babechuk, M.G., Widdowson, M., Kamber, B.S., 2014. Quantifying chemical weathering intensity and trace element release from two contrasting basalt profiles, Deccan Traps, India. Chem. Geol. 363, 56–75. https://doi.org/10.1016/j.chemgeo.2013.10.027.

Bao, J., Song, C., Yang, Y., Fang, X., Meng, Q., Feng, Y., He, P., 2019. Reduced chemical weathering intensity in the Qaidam Basin (NE Tibetan Plateau) during the late Cenozoic. J. Asian Earth Sci. 170, 155–165. https://doi.org/10.1016/j.jseaes.2018.10.018.

Battaglia, S., Leoni, L., Sartori, F., 2003. Mineralogical and grain size composition of clays developing calanchi and biancane erosional landforms. Geomorphology 49 (1–2), 153–170. https://doi.org/10.1016/S0169-555X(02)00171-X.

Bayon, G., Bindeman, I.N., Trinquier, A., Retallack, G.J., Bekker, A., 2022. Long-term evolution of terrestrial weathering and its link to Earth's oxygenation. Earth Planet. Sci. Lett. 584, 117490 https://doi.org/10.1016/j.epsl.2022.117490.

Bengtsson, H., Stevens, R.L., 1998. Source and grain-size influences upon the clay mineral distribution in the Skagerrak and northern Kattegat. Clay Min. 33 (1), 3–13. https://doi.org/10.1016/10.1180/000985598545381.

Berger, G., Lacharpagne, J.C., Velde, B., Beaufort, D., Lanson, B., 1997. Kinetic constraints on illitization reactions and the effects of organic diagenesis in sandstone/shale sequences. Appl. Geochem. 12 (1), 23–35. https://doi.org/10.1016/S0883-2927(96)00051-0.

Biscaye, P.E., 1965. Mineralogy and sedimentation of recent deep-sea clay in the Atlantic Ocean and adjacent seas and oceans. Geol. Soc. Am. Bull. 76 (7), 803–832. https://doi.org/10.1130/0016-7606(1965)76[803:MASORD]2.0.CO;2.

Borchardt, G., 1989. Smectites. In: Minerals in Soil Environments, 1, pp. 675–727.

Bouchez, J., Gaillardet, J., France-Lanord, C., Maurice, L., Dutra-Maia, P., 2011. Grain size control of river suspended sediment geochemistry: Clues from Amazon River depth profiles. Geochem. Geophys. Geosyst. 12, Q03008. https://doi.org/10.1029/2010GC003380.

Buggle, B., Glaser, B., Hambach, U., Gerasimenkoc, N., Marković, S., 2011. An evaluation of geochemical weathering indices in loess–paleosol studies. Quat. Int. 240 (1–2), 12–21. https://doi.org/10.1016/j.quaint.2010.07.019.

Burke, B.C., Heimsath, A.M., White, A.F., 2007. Coupling chemical weathering with soil production across soil-mantled landscapes. Earth Surf. Process. Landf. 32 (6), 853–873. https://doi.org/10.1002/esp.1443.

Cao, L., Shao, L., Qiao, P., Chen, S., Wu, M., 2017. Geochemical evolution of Oligocene-Middle Miocene sediments in the deep-water area of the Pearl River Mouth Basin, northern South China Sea. Mar. Pet. Geol. 80, 358–368. https://doi.org/10.1016/j.marpetgeo.2016.12.010.

Cao, Y., Song, H., Algeo, T.J., Chu, D., Du, Y., Tian, L., Wang, Y., Tong, J., 2019. Intensified chemical weathering during the Permian-Triassic transition recorded in terrestrial and marine successions. Paleogeogr. Paleoclimatol. Paleoecol. 519, 166–177. https://doi.org/10.1016/j.palaeo.2018.06.012.
Caracciolo, L., Tolosana-Delgado, R., Le Pera, E., Von Eynatten, H., Arribas, J., Tarquini, S., 2012. Influence of granitoid textural parameters on sediment composition: implications for sediment generation. Sediment. Geol. 280, 93–107. https://doi.org/10.1016/j.sedgeo.2012.07.005.
Carriquiry, J.D., Sánchez, A., Camacho-Ibar, V.F., 2001. Sedimentation in the northern Gulf of California after cessation of the Colorado River discharge. Sediment. Geol. 144 (1–2), 37–62. https://doi.org/10.1016/S0037-0738(01)00134-8.
Chang, H., An, Z., Wu, F., Jin, Z., Liu, W., Song, Y., 2013. A Rb/Sr record of the weathering response to environmental changes in westerly winds across the Tarim Basin in the late Miocene to the early Pleistocene. Paleogeogr. Paleoclimatol. Paleoecol. 386, 364–373. https://doi.org/10.1016/j.palaeo.2013.06.006.
Chaudhri, A.R., Singh, M., 2012. Clay minerals as climate change indicators—a case study. Am. J. Clim. Chang. 1 (04), 231. https://doi.org/10.4236/ajcc.2012.14020.
Chen, J., Guo, Y., Wei, H.B., Liu, H.Y., Ma, R.Y., Xiao, Z., Feng, Z., 2022. Evaluation of chemical weathering proxies by comparing drilled cores versus outcrops and weathering history during the Permian-Triassic transition. Glob. Planet. Change. 214, 103855 https://doi.org/10.1016/j.gloplacha.2022.103855.
Chen, L., Jin, X., Chen, H., He, Z., Qiu, L., Duan, H., 2020. Grain size distribution and clay mineral distinction of rare earth ore through different methods. Minerals 10 (4), 353. https://doi.org/10.3390/min10040353.
Chen, Q., Li, Z., Dong, S., Yu, Q., Zhang, C., Yu, X., 2021. Applicability of chemical weathering indices of eolian sands from the deserts in northern China. Catena 198, 105032. https://doi.org/10.1016/j.catena.2020.105032.
Chen, X., Zhang, Y., Huo, H., Wu, Z., 2020. Study of high tensile strength of natural continuous basalt fibers. J. Nat. Fibers 17 (2), 214–222. https://doi.org/10.1080/15440478.2018.1477087.
Chen, Y., Hedding, D.W., Li, X., Greyling, A.C., Li, G., 2020. Weathering dynamics of large Igneous Provinces (LIPs): a case study from the Lesotho Highlands. Earth Planet. Sci. Lett. 530, 115871 https://doi.org/10.1016/j.epsl.2019.115871.
Chen, Z., Ding, Z., Yang, S., Sun, J., Zhu, M., Xiao, Y., Tong, F., Liang, Y., 2023. Strong Coupling between Carbon Cycle, climate, and Weathering during the Paleocene-Eocene thermal Maximum. Geophys. Res. Lett. 50 (9), e2023GL102897 https://doi.org/10.1029/2023GL102897.
Chetelat, B., Liu, C.Q., Wang, Q., Zhang, G., 2013. Assessing the influence of lithology on weathering indices of Changjiang river sediments. Chem. Geol. 359, 108–115. https://doi.org/10.1016/j.chemgeo.2013.09.018.
Clift, P.D., Wan, S., Blusztajn, J., 2014. Reconstructing chemical weathering, physical erosion and monsoon intensity since 25 Ma in the northern South China Sea: a review of competing proxies. Earth-Sci. Rev. 130, 86–102. https://doi.org/10.1016/j.earscirev.2014.01.002.
Cox, R., Lowe, D.R., Cullers, R.L., 1995. The influence of sediment recycling and basement composition on evolution of mudrock chemistry in the southwestern United States. Geochim. Cosmochim. Acta 59 (14), 2919–2940. https://doi.org/10.1016/0016-7037(95)00185-9.
Cruz, A., Dinis, P.A., Gomes, A., Leite, P., 2021. Influence of Sediment Cycling on the Rare-Earth Element Geochemistry of Fluvial Deposits (Caculuvar–Mucope, Cunene River Basin, Angola). Geosciences 11 (9), 384. https://doi.org/10.3390/geosciences11090384.
Cuadros, J., 2006. Modeling of smectite illitization in burial diagenesis environments. Geochim. Cosmochim. Acta 70 (16), 4181–4195. https://doi.org/10.1016/j.gca.2006.06.1372.
Dai, X., Du, Y., Ziegler, M., Wang, C., Ma, Q., Chai, R., Guo, H., 2022. Middle Triassic to late Jurassic climate change on the northern margin of the South China Plate: Insights from chemical weathering indices and clay mineralogy. Paleogeogr. Paleoclimatol. Paleoecol. 585, 110744 https://doi.org/10.1016/j.palaeo.2021.110744.
Deepthy, R., Balakrishnan, S., 2005. Climatic control on clay mineral formation: evidence from weathering profiles developed on either side of the Western Ghats. J. Earth Syst. Sci. 114 (5), 545–556. https://doi.org/10.1007/BF02702030.
Dellinger, M., Bouchez, J., Gaillardet, J., Faure, L., Moureau, J., 2017. Tracing weathering regimes using the lithium isotope composition of detrital sediments. Geology 45 (5), 411–414. https://doi.org/10.1130/G38671.1.
Dellisanti, F., Pini, G.A., Baudin, F., 2010. Use of Tmax as a thermal maturity indicator in orogenic successions and comparison with clay mineral evolution. Clay Miner. 45 (1), 115–130. https://doi.org/10.1180/claymin.2010.045.1.115.
Deng, K., Yang, S., Guo, Y., 2022. A global temperature control of silicate weathering intensity. Nat. Commun. 13 (1), 1–10. https://doi.org/10.1038/s41467-022-29415-0.
Di Stefano, C., Ferro, V., Mirabile, S., 2010. Comparison between grain-size analyses using laser diffraction and sedimentation methods. Biosyst. Eng. 106 (2), 205–215. https://doi.org/10.1016/j.biosystemseng.2010.03.013.
Dianto, A., Subehi, L., Ridwansyah, I., Hantoro, W.S., 2019. Clay minerals in the sediments as useful paleoclimate proxy: Lake Sentarum case study, West Kalimantan, Indonesia. In: IOP Conference Series: Earth and Environmental Science, 311. IOP Publishing, p. 012036. https://doi.org/10.1088/1755-1315/311/1/012036.
Dill, H.G., 2020. A geological and mineralogical review of clay mineral deposits and phyllosilicate ore guides in Central Europe–A function of geodynamics and climate change. Ore Geol. Rev. 119, 103304 https://doi.org/10.1016/j.oregeorev.2019.103304.
Dinis, P.A., Garzanti, E., Hahn, A., Vermeesch, P., Cabral-Pinto, M., 2020. Weathering indices as climate proxies. A step forward based on Congo and SW african river muds. Earth-Sci. Rev. 201, 103039 https://doi.org/10.1016/j.earscirev.2019.103039.
Dinis, P., Garzanti, E., Vermeesch, P., Huvi, J., 2017. Climatic zonation and weathering control on sediment composition (Angola). Chem. Geol. 467, 110–121. https://doi.org/10.1016/j.chemgeo.2017.07.030.
Dixon, J.L., Hartshorn, A.S., Heimsath, A.M., DiBiase, R.A., Whipple, K.X., 2012. Chemical weathering response to tectonic forcing: A soils perspective from the San Gabriel Mountains, California. Earth Planet. Sci. Lett. 323, 40–49. https://doi.org/10.1016/j.epsl.2012.01.010.
Dowey, P.J., Taylor, K.G., 2020. Diagenetic mineral development within the Upper Jurassic Haynesville-Bossier Shale, USA. Sedimentology 67 (1), 47–77. https://doi.org/10.1111/sed.12624.
Egli, M., Fitze, P., Mirabella, A., 2001. Weathering and evolution of soils formed on granitic, glacial deposits: results from chronosequences of swiss alpine environments. Catena 45 (1), 19–47. https://doi.org/10.1016/S0341-8162(01)00138-2.
Ehrmann, W., 1998. Implications of late Eocene to early Miocene clay mineral assemblages in McMurdo Sound (Ross Sea, Antarctica) on paleoclimate and ice dynamics. Palaeogeogr. Palaeoclimatol. Palaeoecol. 139 (3–4), 213–231. https://doi.org/10.1016/S0031-0182(97)00138-7.
Emberson, R., Hovius, N., Galy, A., Marc, O., 2016. Chemical weathering in active mountain belts controlled by stochastic bedrock landsliding. Nat. Geosci. 9 (1), 42–45. https://doi.org/10.1038/ngeo2600.
Esquevin, J., 1969. Influence de la composition chimique des illites Sur leur cristalliniťe. Bull. Centre Rech. Pau-SNPA 3 (1), 147–153.
Etemad-Saeed, N.A., Hosseini-Barzi, M.A., Armstrong-Altrin, J.S., 2011. Petrography and geochemistry of clastic sedimentary rocks as evidences for provenance of the Lower Cambrian Lalun Formation, Posht-e-badam block, Central Iran. J. Afr. Earth Sci. 61 (2), 142–159. https://doi.org/10.1016/j.jafrearsci.2011.06.003.
Fagel, N., 2007. Chapter four clay minerals, deep circulation and climate. Dev. Marine Geol. 1, 139–184. https://doi.org/10.1016/S1572-5480(07)01009-3.
Fedo, C.M., Nesbitt, H.W., Young, G.M., 1995. Unraveling the effects of potassium metasomatism in sedimentary rocks and paleosols, with implications for paleoweathering conditions and provenance. Geology 23 (10), 921–924. https://doi.org/10.1130/0091-7613(1995)023<0921:UTEOPM>2.3.CO;2.
Fedo, C.M., Eriksson, K.A., Krogstad, E.J., 1996. Geochemistry of shales from the Archean (~ 3.0 Ga) Buhwa Greenstone Belt, Zimbabwe: implications for provenance and source-area weathering. Geochim. Cosmochim. Acta 60 (10), 1751–1763.
Ferrier, K.L., Riebe, C.S., Hahm, W.J., 2016. Testing for supply-limited and kinetic-limited chemical erosion in field measurements of regolith production and chemical depletion. Geochem. Geophys. Geosyst. 17 (6), 2270–2285. https://doi.org/10.1002/2016gc006273.
Fu, H., Jian, X., Liang, H., Zhang, W., Shen, X., Wang, L., 2022. Tectonic and climatic forcing of chemical weathering intensity in the northeastern Tibetan Plateau since the middle Miocene. Catena 208, 105785. https://doi.org/10.1016/j.catena.2021.105785.
Gabet, E.J., Mudd, S.M., 2009. A theoretical model coupling chemical weathering rates with denudation rates. Geology 37 (2), 151–154. https://doi.org/10.1130/G25270A.1.
Gaillardet, J., Dupré, B., Allègre, C.J., 1999. Geochemistry of large river suspended sediments: silicate weathering or recycling tracer? Geochim. Cosmochim. Acta 63 (23–24), 4037–4051. https://doi.org/10.1016/S0016-7037(99)00307-5.
Galán, E., 2006. Genesis of clay minerals. Dev. Clay Sci. 1, 1129–1162. https://doi.org/10.1016/S1572-4352(05)01042-1.
Garzanti, E., 2019. Petrographic classification of sand and sandstone. Earth-Sci. Rev. 192, 545–563. https://doi.org/10.1016/j.earscirev.2018.12.014.
Garzanti, E., Andò, S., 2019. Heavy minerals for junior woodchucks. Minerals 9 (3), 148. https://doi.org/10.3390/min9030148.
Garzanti, E., Ando, S., France-Lanord, C., Censi, P., Vignola, P., Galy, V., Lupker, M., 2011. Mineralogical and chemical variability of fluvial sediments: 2. Suspended-load silt (Ganga–Brahmaputra, Bangladesh). Earth Planet. Sci. Lett. 302, 107–120. https://doi.org/10.1016/j.epsl.2010.11.043.
Garzanti, E., Ando, S., France-Lanord, C., Vezzoli, G., Censi, P., Galy, V., Najman, Y., 2010. Mineralogical and chemical variability of fluvial sediments 1. Bedload sand (Ganga– Brahmaputra, Bangladesh). Earth Planet. Sci. Lett. 299, 368–381. https://doi.org/10.1016/j.epsl.2010.09.017.
Garzanti, E., Dinis, P., Vermeesch, P., Andò, S., Hahn, A., Huvi, J., Limonta, M., Padoana, M., Resentinia, A., Rittnerc, M., Vezzoli, G., 2018. Dynamic uplift, recycling, and climate control on the petrology of passive-margin sand (Angola). Sediment. Geol. 375, 86–104. https://doi.org/10.1016/j.sedgeo.2017.12.009.
Garzanti, E., He, J., Barbarano, M., Resentini, A., Li, C., Yang, L., Yang, S., Wang, H., 2021. Provenance versus weathering control on sediment composition in tropical monsoonal climate (South China)-2. Sand petrology and heavy minerals. Chem. Geol. 564, 119997 https://doi.org/10.1016/j.chemgeo.2020.119997.
Garzanti, E., Padoan, M., Andò, S., Resentini, A., Vezzoli, G., Lustrino, M., 2013a. Weathering and relative durability of detrital minerals in equatorial climate: sand petrology and geochemistry in the East African Rift. J. Geol. 121 (6), 547–580. https://doi.org/10.1086/673259.
Garzanti, E., Padoan, M., Setti, M., López-Galindo, A., Villa, I.M., 2014. Provenance versus weathering control on the composition of tropical river mud (southern Africa). Chem. Geol. 366, 61–74. https://doi.org/10.1016/j.chemgeo.2013.12.016.
Garzanti, E., Padoan, M., Setti, M., Najman, Y., Peruta, L., Villa, I.M., 2013b. Weathering geochemistry and Sr-Nd fingerprints of equatorial upper Nile and Congo muds. Geochem. Geophys. Geosyst. 14, 292–316. https://doi.org/10.1002/ggge.20060.

Garzanti, E., Resentini, A., 2016. Provenance control on chemical indices of weathering (Taiwan river sands). Sediment. Geol. 336, 81–95. https://doi.org/10.1016/j.sedgeo.2015.06.013.

Garzanti, E., Vermeesch, P., Vezzoli, G., Andò, S., Botti, E., Limonta, M., Dinis, P., Hahn, A., Baudet, D., De Grave, J., Yaya, N.K., 2019. Congo River sand and the equatorial quartz factory. Earth-Sci. Rev. 197, 102918 https://doi.org/10.1016/j.earscirev.2019.102918.

Gibbs, R.J., 1977. Clay mineral segregation in the marine environment. J. Sediment. Res. 47 (1), 237–243. https://doi.org/10.1306/212F713A-2B24-11D7-8648000102C1865D.

Gong, Y., Zeng, Z., Zhou, C., Nan, X., Yu, H., Lu, Y., Li, W., Gou, W., Cheng, W., Huang, F., 2019. Barium isotopic fractionation in latosol developed from strongly weathered basalt. Sci. Total Environ. 687, 1295–1304. https://doi.org/10.1016/j.scitotenv.2019.05.427.

Greber, N.D., Dauphas, N., 2019. The chemistry of fine-grained terrigenous sediments reveals a chemically evolved Paleoarchean emerged crust. Geochim. Cosmochim. Acta 255, 247–264. https://doi.org/10.1016/j.gca.2019.04.012.

Gromet, L.P., Haskin, L.A., Korotev, R.L., Dymek, R.F., 1984. The "North american shale composite": its compilation, major and trace element characteristics. Geochim. Cosmochim. Acta 48 (12), 2469–2482.

Guo, Y., Yang, S., Deng, K., 2021. Disentangle the hydrodynamic sorting and lithology effects on sediment weathering signals. Chem. Geol. 586, 120607 https://doi.org/10.1016/j.chemgeo.2021.120607.

Guo, Y., Yang, S., Li, C., Bi, L., Zhao, Y., 2017. Sediment recycling and indication of weathering proxies. Acta Geochim. 36 (3), 498–501. https://doi.org/10.1007/s11631-017-0218-7.

Guo, Y., Yang, S., Su, N., Li, C., Yin, P., Wang, Z., 2018. Revisiting the effects of hydrodynamic sorting and sedimentary recycling on chemical weathering indices. Geochim. Cosmochim. Acta 227, 48–63. https://doi.org/10.1016/j.gca.2018.02.015.

Gupta, A.S., Rao, S.K., 2001. Weathering indices and their applicability for crystalline rocks. Bull. Eng. Geol. Environ. 60 (3), 201–221. https://doi.org/10.1007/s100640100113.

Harnois, L., 1988. The CIW index: a new chemical index of weathering. Sediment. Geol. 55 (3), 319–322. https://doi.org/10.1016/0037-0738(88)90137-6.

He, J., Garzanti, E., Dinis, P., Yang, S., Wang, H., 2020. Provenance versus weathering control on sediment composition in tropical monsoonal climate (South China)-1. Geochem. Clay Mineral. Chem. Geol. 558, 119860 https://doi.org/10.1016/j.chemgeo.2020.119860.

Hossain, H.Z., Kawahata, H., Roser, B.P., Sampei, Y., Manaka, T., Otani, S., 2017. Geochemical characteristics of modern river sediments in Myanmar and Thailand: implications for provenance and weathering. Geochemistry 77 (3), 443–458. https://doi.org/10.1016/j.chemer.2017.07.005.

Hren, M.T., Hilley, G.E., Chamberlain, C.P., 2007. The relationship between tectonic uplift and chemical weathering rates in the Washington Cascades: field measurements and model predictions. Am. J. Sci. 307 (9), 1041–1063. https://doi.org/10.2475/09.2007.01.

Hu, D., Clift, P.D., Wan, S., Böning, P., Hannigan, R., Hillier, S., Blusztajn, J., 2016. Testing chemical weathering proxies in Miocene-recent fluvial-derived sediments in the South China Sea. Geol. Soc. Lond., Spec. Publ. 429 (1), 45–72. https://doi.org/10.1144/SP429.5.

Huang, J., Jiao, W., Liu, J., Wan, S., Xiong, Z., Zhang, J., Yang, Z., Li, A., Li, T., 2021. Sediment distribution and dispersal in the southern South China Sea: evidence from clay minerals and magnetic properties. Mar. Geol. 439, 106560 https://doi.org/10.1016/j.margeo.2021.106560.

Jaboyedoff, M., Bussy, F., Kubler, B., Thelin, P., 2001. Illite "crystallinity" revisited. Clay Clay Miner. 49 (2), 156–167.

Ji, H., Wang, S., Ouyang, Z., Zhang, S., Sun, C., Liu, X., Zhou, D., 2004. Geochemistry of red residua underlying dolomites in karst terrains of Yunnan-Guizhou Plateau: I. The formation of the Pingba profile. Chem. Geol. 203 (1–2), 1–27. https://doi.org/10.1016/j.chemgeo.2003.08.012.

Jian, X., Guan, P., Zhang, W., Feng, F., 2013. Geochemistry of Mesozoic and Cenozoic sediments in the northern Qaidam basin, northeastern Tibetan Plateau: implications for provenance and weathering. Chem. Geol. 360, 74–88. https://doi.org/10.1016/j.chemgeo.2013.10.011.

Jian, X., Yang, S., Hong, D., Liang, H., Zhang, S., Fu, H., Zhang, W., 2020. Seasonal geochemical heterogeneity of sediments from a subtropical mountainous river in SE China. Mar. Geol. 422, 106120 https://doi.org/10.1016/j.margeo.2020.106120.

Jian, X., Zhang, W., Liang, H., Guan, P., Fu, L., 2019. Mineralogy, petrography and geochemistry of an early Eocene weathering profile on basement granodiorite of Qaidam basin, northern Tibet: Tectonic and paleoclimatic implications. Catena 172, 54–64. https://doi.org/10.1016/j.catena.2018.07.029.

Jin, Z., Cao, J., Wu, J., Wang, S., 2006. A Rb/Sr record of catchment weathering response to Holocene climate change in Inner Mongolia. Earth Surf. Proces. Landf. 31 (3), 285–291. https://doi.org/10.1002/esp.1243.

Joo, Y.J., Madden, M.E., Soreghan, G.S., 2018. Anomalously low chemical weathering in fluvial sediment of a tropical watershed (Puerto Rico). Geology 46 (8), 691–694. https://doi.org/10.1130/G40315.1.

Kafy, R.H., Tobia, F.H., 2022. Geochemical signatures of provenance, chemical weathering, and tectonic setting in the Greater Zab River sediments, Iraqi Kurdistan Region. Arab. J. Geosci. 15 (19), 1–22. https://doi.org/10.1007/s12517-022-10823-x.

Kamp, P.C., 2010. Arkose, subarkose, quartz sand, and associated muds derived from felsic plutonic rocks in glacial to tropical humid climates. J. Sediment. Res. 80 (10), 895–918. https://doi.org/10.2110/jsr.2010.081.

Keller, W.D., 1970. Environmental aspects of clay minerals. J. Sediment. Res. 40 (3), 788–813.

Lai, J., Wang, G., Huang, L., Li, W., Ran, Y., Wang, D., Zhou, Z.L., Chen, J., 2015. Brittleness index estimation in a tight shaly sandstone reservoir using well logs. J. Nat. Gas Sci. Eng. 27, 1536–1545. https://doi.org/10.1016/j.jngse.2015.10.020.

Lanson, B., Beaufort, D., Berger, G., Bauer, A., Cassagnabere, A., Meunier, A., 2002. Authigenic kaolin and illitic minerals during burial diagenesis of sandstones: a review. Clay Min. 37 (1), 1–22. https://doi.org/10.1180/0009855023710014.

Larsen, I.J., Almond, P.C., Eger, A., Stone, J.O., Montgomery, D.R., Malcolm, B., 2014. Rapid soil production and weathering in the Southern Alps, New Zealand. Science 343 (6171), 637–640. https://doi.org/10.1126/science.1244908.

Le Pera, E., Sorriso-Valvo, M., 2000. Weathering and morphogenesis in a Mediterranean climate, Calabria, Italy. Geomorphology 34 (3–4), 251–270. https://doi.org/10.1016/S0169-555X(00)00012-X.

Lee, S.Y., Kim, S.J., Baik, M.H., 2008. Chemical weathering of granite under acid rainfall environment, Korea. Environ. Geol. 55 (4), 853–862. https://doi.org/10.1007/s00254-007-1037-7.

Li, C., Yang, S., 2010. Is chemical index of alteration (CIA) a reliable proxy for chemical weathering in global drainage basins? Am. J. Sci. 310 (2), 111–127. https://doi.org/10.2475/02.2010.03.

Li, F., Yang, S., Breecker, D.O., Ramos, E.J., Huang, X., Duan, Z., Guo, Y.L., Li, C., Mei, X., 2022. Responses of silicate weathering intensity to the Pliocene-Quaternary cooling in East and Southeast Asia. Earth Planet. Sci. Lett. 578, 117301 https://doi.org/10.1016/j.epsl.2021.117301.

Li, M.L., Tian, J., Chen, L., Xu, H., Zheng, D., Liu, W., 2019. New Zircon U-Pb Age and its Restriction on the Warming Time of the Interglacial Paleoclimate during the Cryogenian in the Yangtze Block. J. Geol. 127 (6), 691–701. https://doi.org/10.1086/705327.

Li, M.Y., Zhu, R., Lou, Z., Yin, W., Hu, Z., Zhu, H., Jin, A., 2019. Diagenesis and its impact on the reservoir quality of the fourth member of Xujiahe Formation, Western Sichuan Depression, China. Mar. Pet. Geol. 103, 485–498. https://doi.org/10.1016/j.marpetgeo.2019.03.011.

Li, S., Li, W., Beard, B.L., Raymo, M.E., Wang, X., Chen, Y., Chen, J., 2019. K isotopes as a tracer for continental weathering and geological K cycling. Proc. Natl. Acad. Sci. 116 (18), 8740–8745. https://doi.org/10.1073/pnas.1811282116.

Li, X., Gao, Z., Fang, S., Ren, C., Yang, K., Wang, F., 2019. Fractal characterization of nanopore structure in shale, tight sandstone and mudstone from the Ordos Basin of China using nitrogen adsorption. Energies 12 (4), 583. https://doi.org/10.3390/en12040583.

Li, X., Huang, Y., Zhang, Z., Wang, C., Yang, T., 2022. Orbitally forced chemical weathering in the late cretaceous northeastern China: Implications for paleoclimate change. Glob. Planet. Change. 218, 103982 https://doi.org/10.1016/j.gloplacha.2022.103982.

Liang, F., Niu, J., Linsel, A., Hinderer, M., Scheuvens, D., Petschick, R., 2021. Rock alteration at the post-Variscan nonconformity: implications for Carboniferous-Permian surface weathering versus burial diagenesis and paleoclimate evaluation. Solid Earth 12 (5), 1165–1184. https://doi.org/10.5194/se-12-1165-2021.

Liang, L., Sun, Y., Beets, C.J., Prins, M.A., Wu, F., Vandenberghe, J., 2013. Impacts of grain size sorting and chemical weathering on the geochemistry of Jingyuan loess in the northwestern Chinese Loess Plateau. J. Asian Earth Sci. 69, 177–184. https://doi.org/10.1016/j.jseaes.2012.12.015.

Lin, X., Zhang, Z., Liu, X., Chen, N., Wu, T., Zhang, Y., Zhao, P., Ma, X., Zhou, Z., 2020. Geochemical characteristics of late Triassic sandstones in the western part of Bayan Har Basin, Northern Tibetan Plateau, Western China: Constraints on provenance, source weathering, tectonic setting, and palaeoenvironment. Geol. J. 55 (7), 5275–5293. https://doi.org/10.1002/gj.3743.

Liu, W., Liu, C., Brantley, S.L., Xu, Z., Zhao, T., Liu, T., Yu, C., Xue, D., Zhao, Z., Cui, L., Zhang, Z., Fan, B., Gu, X., 2016. Deep weathering along a granite ridgeline in a subtropical climate. Chem. Geol. 427, 17–34. https://doi.org/10.1016/j.chemgeo.2016.02.014.

Liu, Y., Song, C., Meng, Q., He, P., Yang, R., Huang, R., Chen, S., Wang, D., Xing, Z., 2020. Paleoclimate change since the Miocene inferred from clay-mineral records of the Jiuquan Basin, NW China. Paleogeogr. Paleoclimatol. Paleoecol. 550, 109730 https://doi.org/10.1016/j.palaeo.2020.109730.

Liu, Z., Dreybrodt, W., Liu, H., 2011. Atmospheric CO2 sink: silicate weathering or carbonate weathering? Appl. Geochem. 26, S292–S294. https://doi.org/10.1016/j.apgeochem.2011.03.085.

Liu, Z., Wang, H., Hantoro, W.S., Sathiamurthy, E., Colin, C., Zhao, Y., Li, J., 2012. Climatic and tectonic controls on chemical weathering in tropical Southeast Asia (Malay Peninsula, Borneo, and Sumatra). Chem. Geol. 291, 1–12. https://doi.org/10.1016/j.chemgeo.2011.11.015.

Liu, Z., Zhao, Y., Colin, C., Stattegger, K., Wiesner, M.G., Huh, C.A., Zhang, Y., Li, X., Sompongchaiyakul, P., You, C., Huang, C., Liu, J., Siringan, F., Le, K., Sathiamurthy, E., Hantoro, W., Liu, J., Tuo, S., Zhao, S., Zhou, S., He, Z., Wang, Y., Bunsomboonsakul, S., Li, Y., 2016. Source-to-sink transport processes of fluvial sediments in the South China Sea. Earth-Sci. Rev. 153, 238–273. https://doi.org/10.1016/j.earscirev.2015.08.005.

Locsey, K.L., Grigorescu, M., Cox, M.E., 2012. Water–rock interactions: an investigation of the relationships between mineralogy and groundwater composition and flow in a subtropical basalt aquifer. Aquat. Geochem. 18 (1), 45–75. https://doi.org/10.1007/s10498-011-9148-x.

Lupker, M., France-Lanord, C., Galy, V., Lavé, J., Kudrass, H., 2013. Increasing chemical weathering in the Himalayan system since the last Glacial Maximum. Earth Planet. Sci. Lett. 365, 243–252. https://doi.org/10.1016/j.epsl.2013.01.038.

Lv, D., Wang, L., Isbell, J.L., Lu, C., Li, P., Wang, Y., Zhang, Z., 2022. Records of chemical weathering and volcanism linked to paleoclimate transition during the late Paleozoic

Icehouse. Glob. Planet. Change. 217, 103934 https://doi.org/10.1016/j.gloplacha.2022.103934.
Ma, J.L., Wei, G.J., Xu, Y.G., Long, W.G., Sun, W.D., 2007. Mobilization and re-distribution of major and trace elements during extreme weathering of basalt in Hainan Island, South China. Geochim. Cosmochim. Acta. 71 (13), 3223–3237. https://doi.org/10.1016/j.gca.2007.03.035.
Ma, W., Cao, Y., Xi, K., Liu, K., Lin, M., Liu, J., 2022. Interactions between mineral evolution and organic acids dissolved in bitumen in hybrid shale system. Int. J. Coal Geol. 260, 104071 https://doi.org/10.1016/j.coal.2022.104071.
Maher, K., Chamberlain, C.P., 2014. Hydrologic regulation of chemical weathering and the geologic carbon cycle. Science 343 (6178), 1502–1504. https://doi.org/10.1126/science.1250770.
Mao, H.R., Cui, L.F., Zhang, Z.J., Xu, S., Liu, C.Q., Zhao, Z.Q., 2022. Influence of monsoon climate on chemical weathering of granitic regoliths. Glob. Biogeochem. Cycle. 36 (5), e2022GB007362 https://doi.org/10.1029/2022GB007362.
McLennan, S.M., 1993. Weathering and global denudation. J. Geol. 101 (2), 295–303. https://doi.org/10.1086/648222.
McLennan, S.M., Hemming, S.R., Taylor, S.R., Eriksson, K.A., 1995. Early Proterozoic crustal evolution: Geochemical and NdPb isotopic evidence from metasedimentary rocks, southwestern North America. Geochim. Cosmochim. Acta 59 (6), 1153–1177. https://doi.org/10.1016/0016-7037(95)00032-U.
Mei, H., Jian, X., Zhang, W., Fu, H., Zhang, S., 2021. Behavioral differences between weathering and pedogenesis in a subtropical humid granitic terrain: Implications for chemical weathering intensity evaluation. Catena 203, 105368. https://doi.org/10.1016/j.catena.2021.105368.
Mikesell, L.R., Schaetzl, R.J., Velbel, M.A., 2004. Hornblende etching and quartz/feldspar ratios as weathering and soil development indicators in some Michigan soils. Quat. Res. 62 (2), 162–171. https://doi.org/10.1016/j.yqres.2004.06.006.
Millot, R., Gaillardet, J., Dupré, B., Allègre, C.J., 2002. The global control of silicate weathering rates and the coupling with physical erosion: new insights from rivers of the Canadian Shield. Earth Planet. Sci. Lett. 196 (1–2), 83–98. https://doi.org/10.1016/S0012-821X(01)00599-4.
Millot, R., Tremosa, J., Négrel, P., 2019. Chemical weathering of a granitic watershed: coupling Lithium isotopes and reactive transport modeling, preliminary results[C]// E3S Web of Conferences. EDP Sci. 98, 12014. https://doi.org/10.1051/e3sconf/20199812014.
Minyuk, P.S., Borkhodoev, V.Y., Wennrich, V., 2014. Inorganic geochemistry data from Lake El'gygytgyn sediments: marine isotope stages 6–11. Clim. Past 10 (2), 467–485. https://doi.org/10.5194/cp-10-467-2014.
Mir, A.R., Balaram, V., Ganai, J.A., Dar, S.A., Keshav Krishna, A., 2016. Geochemistry of sedimentary rocks from Permian-Triassic boundary sections of Tethys Himalaya: implications for paleo-weathering, provenance, and tectonic setting. Acta Geochim. 35 (4), 428–436. https://doi.org/10.1007/s11631-016-0107-5.
Molina, A., Vanacker, V., Corre, M.D., Veldkamp, E., 2019. Patterns in soil chemical weathering related to topographic gradients and vegetation structure in a high Andean tropical ecosystem. J. Geophys. Res. Earth Surf. 124 (2), 666–685.
Nadłonek, W., Bojakowska, I., 2018. Variability of chemical weathering indices in modern sediments of the Vistula and Odra Rivers, (Poland). Appl. Ecol. Environ. Res. 16, 2453–2473.
Nayak, K., Lin, A.T.S., Huang, K.F., Liu, Z., Babonneau, N., Ratzov, G., Pillutla, R.K., Das, P., Hsu, S.K., 2021. Clay-mineral distribution in recent deep-sea sediments around Taiwan: Implications for sediment dispersal processes. Tectonophysics 814, 228974. https://doi.org/10.1016/j.tecto.2021.228974.
Nesbitt, H.W., Fedo, C.M., Young, G.M., 1997. Quartz and feldspar stability, steady and non-steady-state weathering, and petrogenesis of siliciclastic sands and muds. J. Geol. 105 (2), 173–192. https://doi.org/10.1086/515908.
Nesbitt, H.W., Young, G.M., 1982. Early Proterozoic climates and plate motions inferred from major element chemistry of lutites. Nature 299 (5885), 715–717. https://doi.org/10.1038/299715a0.
Nesbitt, H.W., Young, G.M., 1984. Prediction of some weathering trends of plutonic and volcanic rocks based on thermodynamic and kinetic considerations. Geochim. Cosmochim. Acta 48 (7), 1523–1534. https://doi.org/10.1016/0016-7037(84)90408-3.
Nesbitt, H.W., Young, G.M., 1989. Formation and diagenesis of weathering profiles. J. Geol. 97 (2), 129–147. https://doi.org/10.1086/629290.
Nesbitt, H.W., Young, G.M., 1997. Sedimentation in the venezuelan Basin, circulation in the Caribbean Sea, and onset of Northern Hemisphere glaciation. J. Geol. 105 (5), 531–544. https://doi.org/10.1086/515954.
Nesbitt, H.W., Young, G.M., McLennan, S.M., Keays, R.R., 1996. Effects of chemical weathering and sorting on the petrogenesis of siliciclastic sediments, with implications for provenance studies. J. Geol. 104 (5), 525–542. https://doi.org/10.1086/629850.
Opfergelt, S., Delmelle, P., 2012. Silicon isotopes and continental weathering processes: Assessing controls on Si transfer to the ocean. Compt. Rendus Geosci. 344 (11–12), 723–738. https://doi.org/10.1016/j.crte.2012.09.006.
Opfergelt, S., Georg, R.B., Delvaux, B., Cabidoche, Y.M., Burton, K.W., Halliday, A.N., 2012. Mechanisms of magnesium isotope fractionation in volcanic soil weathering sequences, Guadeloupe. Earth Planet. Sci. Lett. 341, 176–185. https://doi.org/10.1016/j.epsl.2012.06.010.
Pang, H., Pan, B., Garzanti, E., Gao, H., Zhao, X., Chen, D., 2018. Mineralogy and geochemistry of modern Yellow River sediments: Implications for weathering and provenance. Chem. Geol. 488, 76–86. https://doi.org/10.1016/j.chemgeo.2018.04.010.
Parker, A., 1970. An index of weathering for silicate rocks. Geol. Mag. 107, 501–504.
Peketi, A., Mazumdar, A., Pillutla, S.P.K., Rai, V.K., Sawant, B., Chaitanya, A.V.S., 2020. Monsoon rainfall and contrasting source rocks influenced sediment composition of peninsular basins along the east coast of India (western Bay of Bengal). Mar. Pet. Geol. 118, 104433 https://doi.org/10.1016/j.marpetgeo.2020.104433.
Penman, D.E., Rugenstein, J.K.C., Ibarra, D.E., Winnick, M.J., 2020. Silicate weathering as a feedback and forcing in Earth's climate and carbon cycle. Earth-Sci. Rev. 209, 103298 https://doi.org/10.1016/j.earscirev.2020.103298.
Perri, F., 2020. Chemical weathering of crystalline rocks in contrasting climatic conditions using geochemical proxies: an overview. Paleogeogr. Paleoclimatol. Paleoecol. 556, 109873 https://doi.org/10.1016/j.palaeo.2020.109873.
Price, J.R., Velbel, M.A., 2003. Chemical weathering indices applied to weathering profiles developed on heterogeneous felsic metamorphic parent rocks. Chem. Geol. 202 (3–4), 397–416. https://doi.org/10.1016/j.chemgeo.2002.11.001.
Prudêncio, M.I., Braga, M.S., Paquet, H., Waerenborgh, J.C., Pereira, L.C.J., Gouveia, M. A., 2002. Clay mineral assemblages in weathered basalt profiles from central and southern Portugal: climatic significance. Catena 49 (1–2), 77–89. https://doi.org/10.1016/S0341-8162(02)00018-8.
Rateev, M.A., Gorbunova, Z.N., Lisitzyn, A.P., Nosov, G.L., 1969. The distribution of clay minerals in the oceans. Sedimentology 13, 21–43. https://doi.org/10.1111/j.1365-3091.1969.tb01119.x.
Raza, M., Bhardwaj, V.R., Ahmad, A.H.M., Mondal, M.E.A., Khan, A., Khan, M.S., 2010. Provenance and weathering history of Archaean Naharmagra quartzite of Aravalli craton, NW indian shield: Petrographic and geochemical evidence. Geochem. J. 44 (5), 331–345. https://doi.org/10.2343/geochemj.1.0075.
Ren, X., Nie, J., Saylor, J.E., Li, H., Bush, M.A., Horton, B.K., 2019. Provenance control on chemical weathering index of fluvio-lacustrine sediments: Evidence from the Qaidam Basin, NE Tibetan Plateau. Geochem. Geophys. Geosyst. 20 (7), 3216–3224. https://doi.org/10.1029/2019GC008330.
Repasch, M., Scheingross, J.S., Hovius, N., Vieth-Hillebrand, A., Mueller, C.W., Höschen, C., Szupiany, R.N., Sachse, D., 2022. River organic carbon fluxes modulated by hydrodynamic sorting of particulate organic matter. Geophys. Res. Lett. 49 (3), e2021GL096343 https://doi.org/10.1029/2021GL096343.
Riebe, C.S., Hahm, W.J., Brantley, S.L., 2017. Controls on deep critical zone architecture: a historical review and four testable hypotheses. Earth Surf. Process. Landf. 42 (1), 128–156. https://doi.org/10.1002/esp.4052.
Riebe, C.S., Kirchner, J.W., Granger, D.E., Finkel, R.C., 2001. Strong tectonic and weak climatic control of long-term chemical weathering rates. Geology 29 (6), 511–514. https://doi.org/10.1130/0091-7613(2001)029<0511:STAWCC>2.0.CO;2.
Ruxton, B.P., 1968. Measures of the degree of chemical weathering of rocks. J. Geol. 76 (5), 518–527.
Scheffler, K., Buehmann, D., Schwark, L., 2006. Analysis of late Palaeozoic glacial to postglacial sedimentary successions in South Africa by geochemical proxies–Response to climate evolution and sedimentary environment. Paleogeogr. Paleoclimatol. Paleoecol. 240 (1–2), 184–203. https://doi.org/10.1016/j.palaeo.2006.03.059.
Schneider, S., Hornung, J., Hinderer, M., Garzanti, E., 2016. Petrography and geochemistry of modern river sediments in an equatorial environment (Rwenzori Mountains and Albertine rift, Uganda)—Implications for weathering and provenance. Sediment. Geol. 336, 106–119. https://doi.org/10.1016/j.sedgeo.2016.02.006.
Sebastian, T., Nath, B.N., Venkateshwarlu, M., Miriyala, P., Prakash, A., Linsy, P., Kocherla, M., Kazip, A., Sijinkumar, A.V., 2019. Impact of the Indian Summer Monsoon variability on the source area weathering in the Indo-Burman ranges during the last 21 kyr–A sediment record from the Andaman Sea. Paleogeogr. Paleoclimatol. Paleoecol. 516, 22–34. https://doi.org/10.1016/j.palaeo.2018.11.035.
Selvaraj, K., Chen, C.T.A., 2006. Moderate chemical weathering of subtropical Taiwan: constraints from solid-phase geochemistry of sediments and sedimentary rocks. J. Geol. 114 (1), 101–116. https://doi.org/10.1086/498102.
Shao, J., Yang, S., Li, C., 2012. Chemical indices (CIA and WIP) as proxies for integrated chemical weathering in China: inferences from analysis of fluvial sediments. Sediment. Geol. 265, 110–120. https://doi.org/10.1016/j.sedgeo.2012.03.020.
Shao, J.Q., Yang, S.Y., 2012. Does chemical index of alteration (CIA) reflect silicate weathering and monsoonal climate in the Changjiang River basin? Chin. Sci. Bull. 57 (10), 1178–1187. https://doi.org/10.1007/s11434-011-4954-5.
Singh, P., 2009. Major, trace and REE geochemistry of the Ganga River sediments: influence of provenance and sedimentary processes. Chem. Geol. 266 (3–4), 242–255. https://doi.org/10.1016/j.chemgeo.2009.06.013.
Stone, A., Bateman, M.D., Burrough, S.L., Garzanti, E., Limonta, M., Radeff, G., Telfer, M. W., 2019. Using a portable luminescence reader for rapid age assessment of aeolian sediments for reconstructing dunefield landscape evolution in southern Africa. Quat. Geochronol. 49, 57–64. https://doi.org/10.1016/j.quageo.2018.03.002.
Su, N., Yang, S.Y., Wang, X.D., Bi, L., Yang, C.F., 2015. Magnetic parameters indicate the intensity of chemical weathering developed on igneous rocks in China. Catena 133, 328–341. https://doi.org/10.1016/j.catena.2015.06.003.
Sun, S., Chen, A., Chen, H., Hou, M., Yang, S., Xu, S., Wang, F., Huang, Z., Ogg, J.G., 2022. Early Permian chemical weathering indices and paleoclimate transition linked to the end of the coal-forming episode, Ordos Basin, North China Craton. Paleogeogr. Paleoclimatol. Paleoecol. 585, 110743 https://doi.org/10.1016/j.palaeo.2021.110743.
Sun, S., Chen, A., Hou, M., Yang, S., Ogg, J.G., Zou, H., Xu, S., Li, Q., Huang, Y., Li, R., Chen, H., 2022. Rapid climatic fluctuations during the Guadalupian-Lopingian transition: Implications from weathering indices recorded in acid-insoluble residues of carbonate rocks, South China. J. Asian Earth Sci. 230, 105222 https://doi.org/10.1016/j.jseaes.2022.105222.
Sun, S.S., Ao, M., Geng, K.R., Chen, J.Q., Li, J.J., Guan, Z.T., Mo, B., Liu, T., Yang, W., Tang, Y., Qiu, R.L., 2022. Enrichment and speciation of chromium during basalt weathering: Insights from variably weathered profiles in the Leizhou Peninsula,

South China. Sci. Total Environ. 822, 153304 https://doi.org/10.1016/j.scitotenv.2022.153304.
Tan, X., Liu, F., Hu, L., Reed, A.H., Furukawa, Y., Zhang, G., 2017. Evaluation of the particle sizes of four clay minerals. Appl. Clay Sci. 135, 313–324. https://doi.org/10.1016/j.clay.2016.10.012.
Tavakoli, N., Davoudian, A.R., Shabanian, N., Azizi, H., Neubauer, F., Asahara, Y., Bernroider, M., 2020. Zircon U-Pb dating, mineralogy and geochemical characteristics of the gabbro and gabbro-diorite bodies, Boein-Miandasht, western Iran. Int. Geol. Rev. 62 (13–14), 1658–1676. https://doi.org/10.1080/00206814.2019.1583139.
Teng, F.Z., Hu, Y., Ma, J.L., Wei, G.J., Rudnick, R.L., 2020. Potassium isotope fractionation during continental weathering and implications for global K isotopic balance. Geochim. Cosmochim. Acta 278, 261–271. https://doi.org/10.1016/j.gca.2020.02.029.
Tolosana-Delgado, R., von Eynatten, H., 2009. Grain-size control on petrographic composition of sediments: compositional regression and rounded zeros. Math. Geosci. 41 (8), 869–886. https://doi.org/10.1007/s11004-009-9216-6.
Tunçay, T., Dengiz, O., Bayramin, I., Kilic, S., Baskan, O., 2019. Chemical weathering indices applied to soils developed on old lake sediments in a semi-arid region of Turkey. Eur. J. Soil Sci. 8 (1), 60–72. https://doi.org/10.18393/ejss.499122.
Taylor, S.R., McLennan, S.M., 1985. The Continental Crust: Its Composition and Evolution.
Varela, D.E., Pride, C.J., Brzezinski, M.A., 2004. Biological fractionation of silicon isotopes in Southern Ocean surface waters. Glob. Biogeochem. Cycle. 18 (1) https://doi.org/10.1029/2003GB002140.
Varga, A., Újvári, G., Raucsik, B., 2011. Tectonic versus climatic control on the evolution of a loess–paleosol sequence at Beremend, Hungary: an integrated approach based on paleoecological, clay mineralogical, and geochemical data. Quat. Int. 240 (1–2), 71–86. https://doi.org/10.1016/j.quaint.2010.10.032.
von Eynatten, H., 2004. Statistical modelling of compositional trends in sediments. Sediment. Geol. 171 (1–4), 79–89. https://doi.org/10.1016/j.sedgeo.2004.05.011.
von Eynatten, H., Tolosana-Delgado, R., Karius, V., 2012. Sediment generation in modern glacial settings: grain-size and source-rock control on sediment composition. Sediment. Geol. 280, 80–92. https://doi.org/10.1016/j.sedgeo.2012.03.008.
Wang, A., Zhong, D., Zhu, H., Guo, L., Jiang, Y., Yang, X., Xie, R., 2019. Diagentic features of illite in Upper Triassic Chang-7 tight oil sandstones, Ordos Basin. Geosci. J. 23, 281–298. https://doi.org/10.1007/s12303-018-0033-0.
Wang, J., Li, A., Xu, K., Zheng, X., Huang, J., 2015. Clay mineral and grain size studies of sediment provenances and paleoenvironment evolution in the middle Okinawa Trough since 17 ka. Mar. Geol. 366, 49–61. https://doi.org/10.1016/j.margeo.2015.04.007.
Wang, J., Wu, C., Zhou, T., Zhu, W., Li, X., Zhang, T., 2019. Source and sink evolution of a Permian-Triassic rift–drift basin in the southern Central Asian Orogenic Belt: Perspectives on sedimentary geochemistry and heavy mineral analysis. J. Asian Earth Sci. 181, 103905 https://doi.org/10.1016/j.jseaes.2019.103905.
Warr, L.N., 2022. Earth's clay mineral inventory and its climate interaction: a quantitative assessment. Earth-Sci. Rev. 234, 104198 https://doi.org/10.1016/j.earscirev.2022.104198.
West, A.J., Galy, A., Bickle, M., 2005. Tectonic and climatic controls on silicate weathering. Earth Planet. Sci. Lett. 235 (1–2), 211–228. https://doi.org/10.1016/j.epsl.2005.03.020.
White, A.F., Blum, A.E., Schulz, M.S., Bullen, T.D., Harden, J.W., Peterson, M.L., 1996. Chemical weathering rates of a soil chronosequence on granitic alluvium: I. Quantification of mineralogical and surface area changes and calculation of primary silicate reaction rates. Geochim. Cosmochim. Acta 60 (14), 2533–2550. https://doi.org/10.1016/0016-7037(96)00106-8.
White, A.F., Brantley, S.L., 2018. Chemical weathering rates of silicate minerals: an overview. In: White, A.F., Brantley, S.L. (Eds.), Chemical Weathering Rates of Silicate Minerals. De Gruyter, pp. 1–22. https://doi.org/10.1515/9781501509650-003.
Wu, K., Liu, S., Kandasamy, S., Jin, A., Lou, Z., Li, J., Wu, B., Wang, X., Mohamed, C.A., Shi, X., 2019. Grain-size effect on rare earth elements in Pahang River and Kelantan River, Peninsular Malaysia: Implications for sediment provenance in the southern South China Sea. Cont. Shelf Res. 189, 103977 https://doi.org/10.1016/j.csr.2019.103977.
Xie, Y., Yuan, F., Zhan, T., Kang, C., Chi, Y., 2018. Geochemical and isotopic characteristics of sediments for the Hulun Buir Sandy Land, Northeast China: implication for weathering, recycling and dust provenance. Catena 160, 170–184. https://doi.org/10.1016/j.catena.2017.09.008.
Xiong, S., Ding, Z., Zhu, Y., Zhou, R., Lu, H., 2010. A∼ 6 Ma chemical weathering history, the grain size dependence of chemical weathering intensity, and its implications for provenance change of the chinese loess–red clay deposit. Quat. Sci. Rev. 29 (15–16), 1911–1922. https://doi.org/10.1016/j.quascirev.2010.04.009.
Xu, G., Feng, Q., Deconinck, J.F., Shen, J., Zhao, T., Young, A.L., 2017. High-resolution clay mineral and major elemental characterization of a Permian-Triassic terrestrial succession in southwestern China: Diagenetic and paleoclimatic/paleoenvironmental significance. Paleogeogr. Paleoclimatol. Paleoecol. 481, 77–93. https://doi.org/10.1016/j.palaeo.2017.05.027.
Yang, J., Cawood, P.A., Du, Y., Li, W., Yan, J., 2016. Reconstructing early Permian tropical climates from chemical weathering indices. Bulletin 128 (5–6), 739–751. https://doi.org/10.1130/B31371.1.
Yang, S.Y., Li, C.X., Yang, D.Y., Li, X.S., 2004. Chemical weathering of the loess deposits in the lower Changjiang Valley, China, and paleoclimatic implications. Quat. Int. 117 (1), 27–34. https://doi.org/10.1016/S1040-6182(03)00113-7.
Yu, Z., Wan, S., Colin, C., Yan, H., Bonneau, L., Liu, Z., Song, L., Sun, H., Xu, Z., Jiang, X., Li, A., Li, T., 2016. Co-evolution of monsoonal precipitation in East Asia and the tropical Pacific ENSO system since 2.36 Ma: New insights from high-resolution clay mineral records in the West Philippine Sea. Earth Planet. Sci. Lett. 446, 45–55. https://doi.org/10.1016/j.epsl.2016.04.022.
Yusoff, Z.M., Ngwenya, B.T., Parsons, I., 2013. Mobility and fractionation of REEs during deep weathering of geochemically contrasting granites in a tropical setting, Malaysia. Chem. Geol. 349, 71–86. https://doi.org/10.1016/j.chemgeo.2013.04.016.
Yuste, A., Luzón, A., Bauluz, B., 2004. Provenance of Oligocene-Miocene alluvial and fluvial fans of the northern Ebro Basin (NE Spain): an XRD, petrographic and SEM study. Sediment. Geol. 172 (3–4), 251–268. https://doi.org/10.1016/j.sedgeo.2004.10.001.
Zeng, S., Wang, J., Zeng, Y., Song, C., Wang, D., Zhan, W., Sun, W., 2022. Episodic volcanic eruption and arid climate during the Triassic-Jurassic transition in the Qiangtang Basin, eastern Tethys: a possible linkage with the end-Triassic biotic crises. J. Asian Earth Sci. 237, 105345 https://doi.org/10.1016/j.jseaes.2022.105345.
Zhai, L., Wu, C., Ye, Y., Zhang, S., Wang, Y., 2018. Fluctuations in chemical weathering on the Yangtze Block during the Ediacaran-Cambrian transition: Implications for paleoclimatic conditions and the marine carbon cycle. Paleogeogr. Paleoclimatol. Paleoecol. 490, 280–292. https://doi.org/10.1016/j.palaeo.2017.11.006.
Zhang, L., Yan, D., Yang, S., Li, B., Fu, H., Wang, G., Yang, X., Zhang, B., Liang, W., Zhang, J., 2023. Evolution of the Middle Jurassic paleoclimate: Sedimentary evidence from coal-bearing strata in the Santanghu Basin, NW China. J. Asian Earth Sci. 242, 105495 https://doi.org/10.1016/j.jseaes.2022.105495.
Zhang, X., Li, X.L., Garzanti, E., Lin, C.M., Deng, K., 2021. Sedimentary geochemistry response to climate change on a millennial timescale in the Qiantang River incised-valley system, eastern China. Chem. Geol. 586, 120587 https://doi.org/10.1016/j.chemgeo.2021.120587.
Zhang, Z., Ma, J., Wang, Z., Zhang, L., He, X., Zhu, G., Zeng, T., Wei, G., 2021. Rubidium isotope fractionation during chemical weathering of granite. Geochim. Cosmochim. Acta 313, 99–115. https://doi.org/10.1016/j.gca.2021.08.010.
Zhao, M.Y., Zheng, Y.F., 2015. The intensity of chemical weathering: Geochemical constraints from marine detrital sediments of Triassic age in South China. Chem. Geol. 391, 111–122. https://doi.org/10.1016/j.chemgeo.2014.11.004.
Zhou, X., Li, A., Jiang, F., Lu, J., 2015. Effects of grain size distribution on mineralogical and chemical compositions: a case study from size-fractional sediments of the Huanghe (Yellow River) and Changjiang (Yangtze River). Geol. J. 50 (4), 414–433. https://doi.org/10.1002/gj.2546.